



Up to 1-hour forecasting of radiation hazards from solar energetic ion events with relativistic electrons

Arik Posner^{1,2}

Received 11 July 2006; revised 19 December 2006; accepted 4 January 2007; published 25 May 2007.

[1] The sudden and prompt occurrence of solar energetic particle events poses a hazard to manned space activities and interferes with robotic space science missions. This study demonstrates the possibility of short-term forecasting of the appearance and intensity of solar ion events by means of relativistic, near-light speed electrons. A list of the most severe proton events measured by GOES 8 in the years 1996–2002 serves as a basis to derive the fundamentals of the forecasting method with statistical and superposed epoch techniques. The Comprehensive Suprathermal and Energetic Particle Analyzer (COSTEP) on SOHO provides relativistic electron and <50 MeV proton observations at 1 AU. With a subset of solar particle events (SPEs) where the location of the associated flare on the Sun has been determined, we find that (1) relativistic electrons always arrive at 1 AU ahead of nonrelativistic SPEs allowing their forecasting; (2) the intensity increase of both, electrons and protons alike, depends on the magnetic connection, i.e., the magnetic longitude difference between the observer and the flare; and (3) as coming from one source under near-identical propagation conditions, significant correlations exist that show that the early electron intensity and increase can be utilized as a matrix to forecast the upcoming proton intensity. The study demonstrates one initial empirical forecasting technique with electron and proton observations in 2003.

Citation: Posner, A. (2007), Up to 1-hour forecasting of radiation hazards from solar energetic ion events with relativistic electrons, *Space Weather*, 5, S05001, doi:10.1029/2006SW000268.

1. Introduction

[2] Transient enhancements of particles that pose hazards to humans and technology in space [Hoff *et al.*, 2004], termed solar energetic particle (SEP) events, occur in close association with intense solar activity. The hazard predominantly stems from the unpredictability of solar particle events (SPEs) and their often sudden rise in intensity. Most notably, the ground-level event of 20 January 2005 accelerated protons to GeV energies within 5–10 min [Mewaldt *et al.*, 2005a]. At this event, the unshielded blood-forming organ dose rate from protons alone increased to up to 5 cGy-Eq/hr [Kim *et al.*, 2005] within less than 4 hours. Acute radiation effects set in at about 1 cGy/hr.

[3] Van Hollebeke *et al.* [1975] referred to electrons as the first in situ sign of a particle event. Moreover, this study shows that relativistic electrons from SEPs carry important information with them that can be exploited to character-

ize aspects of the risetime and intensity of the later arriving ions. This study demonstrates the possibility of early warning by using the propagation speed advantage of relativistic electrons over ions on their path from the Sun to 1 AU. The relativistic electrons from SEPs, highly abundant and easy to detect outside the magnetosphere, can be used as messengers for the later arriving ions, predominantly protons with energies that affect humans and technology in space. This study sheds light on the forecasting potential behind this technique. It defines the particle type and energy to be warned against. Also, it tests a preliminary forecasting method against false and missed warnings.

[4] Energetic protons and heavier ions are among the main constituents of SEP events and their effects on the human body carry a significantly higher long-term cancer risk than relativistic, minimum-ionizing electrons. The International Commission on Radiation Protection (ICRP) defines a function (e.g., ICRP60) that relates the linear energy transfer (LET) of particles to an empirical quality factor. The quality factor Q is an assigned value for the relative

¹Southwest Research Institute, San Antonio, Texas, USA.

²Also at NASA Headquarters, Washington, D. C., USA.

risk that a particle poses to cause genetic damage that can potentially lead to the development of cancer in the human body. Q varies between 1 (lowest risk) and 30. LET simply describes kinetic energy loss per unit length for ionizing radiation in tissue. Singly charged, fast moving electrons always have the low quality factor $Q = 1$ ($LET < 10 \text{ keV}/\mu\text{m}$), whereas ion quality factors can reach the value $Q = 30$ at $100 \text{ keV}/\mu\text{m}$. It appears necessary to warn of upcoming energetic ion events from the Sun with their high potential of causing long-term risks to astronaut health.

[5] A direct threat to mission success is posed by the acute radiation syndrome with effects such as vomiting, burns of exposed skin, or blindness. The dose rate of ionizing radiation interacting with human tissue, if critical values are reached or exceeded, causes immediate effects. A warning as early as possible, with a method such as the one described below, can mitigate the risk of acute, debilitating radiation damage to astronauts.

[6] The threshold energy of light ions (p , He) that penetrate space suits to reach tissue or even harm the sensitive blood-forming organs in the human body is on the order of 20–40 MeV/n. Similar thresholds ($\sim 10 \text{ MeV/n}$) apply for radiation that penetrates spacecraft (s/c) housing. Heavy ions generally have lower relative penetration power; that is, their range in matter is shorter as compared to protons and helium; thus the threshold energy increases with increasing nuclear charge number.

[7] Having described the lower limit of ion energies posing a threat, it is clear that all higher-energy ions can harm humans in space. In the context of a warning system it is of merit to discuss the upper limit of the energy/speed range for ions that is most useful to be warned against. This limit is determined by the amount of shielding that is available. However, this value might depend strongly on the situation. On the lunar surface, the presence of the regolith or dust can be utilized to build up rather substantially shielded refuges that will even limit the exposure to cosmic rays. In case of human missions in free space, the possibilities are much more limited. The wall thickness necessary for stopping energetic ions increases with ion kinetic energy. As an example, several g/cm^2 of aluminum may shield up to 100 MeV protons. Ions beyond 100 MeV/n are almost impossible to shield against without unreasonable mass penalty for space exploration vehicles.

[8] SEPs frequently reach GeV or cosmic ray energies. Radiation damage prevention in terms of exposure time to high dose rate and total dose saved clearly depends both on the event encountered and the immediate shielding options at hand. Integration over warning time and energy range that includes effects of particle transport through shielding would give an indication whether the total dose saved would be relevant in a worst case scenario. Models and modules such as BRYNTRN [Wilson *et al.*, 1989; Cucinotta *et al.*, 1994] and EMMREM [Schwadron *et al.*, 2006] are becoming more and more sophisticated, but adequate treatment of this problem would exceed the scope of this paper. However, the 20 January 2005 SEP

event has shown that acute effects from high dose rate exposure to protons alone would have been received very early after onset. This is sufficient motivation to pursue rapid in situ SEP radiation forecasting techniques.

[9] Expressions of activity near or on the Sun are flares, coronal mass ejections (CMEs), and solar radio bursts. To date, the 20-year-old debate within the solar and heliospheric community continues on the relative roles that flares and CMEs play in the acceleration and release of SEPs. RHESSI and the upcoming STEREO mission with sophisticated remote sensing and in situ instrumentation will gather more evidence of particle acceleration on the Sun and in the lower corona. At the same time, research employs advanced models to explore the possibilities of effective and fast acceleration of particles associated with flares and bow shocks of CMEs [Emslie *et al.*, 2004; Tylka *et al.*, 2005]. Sections 4.4 and 6.1 tackle the question of whether processes are present in relativistic electron onsets and potentially lead to bimodal sets of characteristics, as this may affect the general applicability of the proposed forecasting technique.

[10] At least two major physical processes have been recognized that accelerate charged particles at or near the Sun: (1) solar flares, including electric fields, magnetic reconnection, and, most recently discovered, contracting magnetic islands [Drake *et al.*, 2006] and (2) shock waves, including coronal and interplanetary shocks, the associated Fermi 1 and 2 processes, and wave-particle interaction. This list of candidate processes is not intended to be complete. So far, only the contracting magnetic island process has been able to address the question why nearly half the energy released in solar eruptions is in form of energetic electrons.

[11] As interplanetary traveling shocks at 1 AU predominantly energize ions, but only moderate amounts of electrons, the method of forecasting ion events is not intended to forecast shock arrivals in situ. There are other techniques, however, intended for predicting the arrival of IP shocks at 1 AU [Cohen *et al.*, 2001; Posner *et al.*, 2004]. Comprehensive Suprathermal and Energetic Particle Analyzer (COSTEP) observations from 1995–2005 show that all hazardous (containing significant fluences of greater than 30 MeV/n ions) solar ion events are accompanied by enhancements in relativistic electrons. Recently, ACE-EPAM investigators interpreted subrelativistic electron observations in the way that a release of protons before electrons (and vice versa) is possible (E. Roelof and D. Haggerty, personal communication, 2006). Further investigations into this subject are necessary before any conclusive statements can be drawn against the prevailing assumption of simultaneous release of electrons and protons onto open field lines near the Sun. Note that a large speed difference leads to relativistic electrons always arriving at 1 AU substantially (tens of minutes, see below) ahead of hazard threshold protons. This effect clearly exceeds any potential delays in the release time, and to date there has never been a solar particle event reported

where $\sim 30\text{--}100$ MeV protons arrived at 1 AU before the onset of relativistic electrons. In the following, simultaneous release of electrons and protons at the Sun is assumed.

[12] In the worst case scenario for astronauts (i.e., zero pitch angle and propagation along an ideal spiral magnetic field line), the speed difference of ions at 30 MeV with the relativistic electrons allows for a minimum of 30.4 min advance warning time, assuming a connection distance of 1.2 AU to the Sun along the interplanetary magnetic field. Looking at protons with higher kinetic energy (velocity), the minimum warning time decreases. 50 MeV/n ions arrive at least 21.8 min after the relativistic electrons, 100 MeV/n ions arrive with a minimum delay of 13.3 min, and 300 MeV/n ions lag behind in excess of 5 min. Nonetheless, typical solar energetic particle fluxes fall off as a power law or exponentials in flux over energy. Given identical fluxes at the 30 MeV/n hazard threshold for ions, the radiation hazard that is posed by the event depends on the spectral index, with hard spectrum events forming the worst case scenario. A softer spectrum is easier to shield against and provides lower primary and secondary ionizing radiation hazards immediately following the electron warning as compared to a hard spectrum event. Nonetheless, the dominating fluxes that drive the (acute) hazard to humans and technology, more so in a soft spectrum event, are always found at the low-energy hazard threshold.

[13] This study shows that the average delay of 30 MeV ions over relativistic electrons is about twice as much (63 min) as under ideal propagation conditions. Extrapolating to higher energies this means that electron warnings leave on average about 30 min advance warning time for the main SEP ion species, protons and helium, at 100 MeV/n.

[14] In this study, an algorithm that warns against $>30\text{--}50$ MeV protons is being tested and achieves on average >30 min warning time before a critical flux level is reached. More sophisticated forecasting may lead to up to 1 hour forecasting in the future.

[15] In order to be relevant for human and robotic explorers, certain criteria need to be met by any operational radiation warning system. The system needs to indicate early and reliably that the radiation will reach the hazard level. In particular, the warning system should neither miss relevant events that exceed the hazard level nor issue false warnings at an unacceptably high rate such that it might be disruptive for space activities.

[16] The term "advance warning" of solar particle hazard, presumably from an operational software connected with a particle detector on a heliospheric spacecraft, is meant as a notification to take immediate action, i.e., taking shelter inside spacecraft or even specific high-shielding areas until the radiation storm has ceased. Although the radiation damage to space systems and long-term effects to humans from energetic electrons (and in some cases relativistic ions) is in most cases less severe than that from upcoming ions near the hazard

threshold energy, it is advised to take precautions immediately upon warning of a severe particle event hazard.

[17] This study shows that local warnings from a radiation monitor mission can cover a small fraction of the heliosphere in longitude only. For example, a monitor in L1, i.e., corotating with the Earth, suffices to cover a small range of heliospheric longitudes containing the Earth-Moon system. Local warnings, when on the surface of a planetary body without an atmosphere and/or outside a magnetosphere on the other hand, would avoid delays from relaying warnings. Potentially, operators on the ground, on the surface of the Moon or in LEO can make their decision to halt or abort launches into unprotected regions in space dependent on the existence of a hazard warning from L1.

[18] As there is always a possibility for false warnings, any confirmation (or lack thereof) of the potential proton event will arise from direct proton measurements from the very same detector within hours after the warning is issued. Such an energetic particle monitor will continuously warn of radiation danger until the in situ particle environment allows for continuation of routine or launch operation. This study furthermore shows that a possibility exists for longer-term warnings, such as a prediction of an average time-intensity profile for severe SPEs.

[19] This paper explores and tests SPE relativistic electron warning signals. In section 2 follows a discussion on the instrumentation used. Recently, studies presented at larger meetings have shown that GOES SEM particle onset studies are commonplace and conclusions have been drawn from these studies despite the cautioning by the GOES particle team. Therefore, as a service to the community, section 3 summarizes SEP-related onset problems of the level 2 differential flux data from GOES 8/SEM and COSTEP. The in-depth analysis is presented in Appendix A. Furthermore, section 3 introduces a technique that allows a direct comparison between particle detectors with overlapping but distinct energy ranges. (The only requirement is the availability of pulse height analyzed data with sufficient statistics in one of the involved particle detectors.)

[20] Section 4 analyzes with statistical and superposed-epoch methods the early risetimes of 1996–2002 solar electron and ion events and their association with the magnetic connection to the flare location and investigates the short-term and longer-term warning potential from 1 AU. Section 5 tests an electron warning method for the year 2003 and the Halloween events in particular. This paper closes with discussing the impact in section 6.

2. Instrumentation

[21] The Electron Proton Helium Instrument (EPHIN) sensor head as part of the Comprehensive Suprathermal and Energetic Particle Analyzer (COSTEP) [Müller-Mellin *et al.*, 1995] consists of six solid-state detectors (SSDs) stacked within active anticoincidence shielding. The instrument is sensitive to particles from the minimum

ionizing range up to ionization densities of stopping He ions. The stopping power from the active detectors sets the energy ranges for relativistic electrons as 150 keV to 10 MeV and energetic ions (p, He) as 4 MeV/n – >54 MeV/n). As such, COSTEP covers several relevant aspects of the solar energetic particle spectrum, including the capability to provide isotopic composition for light elements.

[22] A combination of coincidence depth (i.e., number of subsequent SSDs reached) and energy loss in the front SSD defines the sorting into science channels of COSTEP. All science channels carry fast (μ s) counters. The pulse height analyzed (PHA) data contain additional information with the individual energy losses in up to five detectors for a representative subset (statistical sample) of particles within a channel. Therefore COSTEP provides the necessary information for ground processing to separate electrons and light ion isotopes even in complex mixed-field environments. In addition, COSTEP data allow for the identification of ionizing electromagnetic radiation with providing single detector count rates.

[23] The relatively large geometric factor ($5.1 \text{ cm}^2 \text{ sr}$ for ions) of the COSTEP instrument automatically adapts to harsh radiation conditions. The switching off of the outer rings (5/6 in area) of the two front SSDs achieves a significant lowering of the geometric factor, but it also creates a leak in the anticoincidence shield. COSTEP data are available at <http://www2.physik.uni-kiel.de/SOHO/phpeph/EPHIN.htm>.

[24] For the strongest SEP events it is inevitable that pileup sets in and limits the accuracy and reliability of the instrument. For this reason, we compared COSTEP observations with GOES 8 Space Environment Monitor (SEM) differential flux proton data, obtained from the National Oceanic and Atmospheric Administration (NOAA) web site (<http://spidr2.ngdc.noaa.gov/spidr/index.jsp>) in order to cover the entire solar event spectrum from small to large. We chose the overlap in time of SOHO with GOES 8, 1996–2002 (only full years), for the statistical and superposed epoch analysis study. The GOES 8/SEM instrument consists of SSDs wrapped in passive shielding. The GOES 8 satellite observes from geostationary orbit about the Earth and nominally remains within the Earth's magnetosphere. All electron data used in this study originate from COSTEP, as GOES electron measurements can be highly contaminated by low-energy protons and magnetospheric electrons. The GOES differential flux proton data used here are, for the most part, corrected for the effects of high-energy particles that penetrate the passive shielding. Its strength in covering strong SEP events makes it very attractive to the space science community, where it is generally in circulation for purely scientific, but also space weather applied studies. However, NOAA cautions on its Web site (http://sec.noaa.gov/weekly/Usr_guide.pdf) that cross contamination for the proton detector exists. In particular, the applied correction algorithm removes “background” in lower-energy channels under the assumption that the incident proton spectrum is

a power law in the two channels above. This assumption is violated during the phases of the onsets of SPEs, in particular at times when velocity dispersion affects the channels needed for correction, as it temporarily leads to spectra at 1 AU that increase in intensity with energy.

[25] Ancillary in situ data originate from the Solar Wind Experiment (SWE) [Ogilvie *et al.*, 1995] on the Wind spacecraft. We use SWE solar wind speeds in order to obtain the nominal connection longitude of the magnetic field line along the heliospheric magnetic field on the Sun and for testing events from the GOES 8 event list for in situ shocks. Also, we use remote sensing data of flare X rays observed by the GOES X-ray burst instrument as reported in Solar Geophysical Data. The ACE/EPAM team's <300 keV beamed electron event list is also being used as a reference.

3. Onset-Specific Instrument Limitations for the Use of GOES 8/SEM and SOHO/COSTEP Data

[26] All energetic particle instruments have attributes that limit measurement reliability under adverse circumstances. This section summarizes such problems for GOES 8/SEM and SOHO/COSTEP-EPHIN. Note that a detailed discussion of these problems is fully laid out in Appendix A. Challenges through SEP onsets and main phases impact GOES 8/SEM and SOHO/COSTEP measurements in distinctly different ways.

[27] The COSTEP electron time profile is reliable and accurate throughout most small and intermediate solar energetic particle events. Even for some intense events, such as encountered on 4 November 2001 (Figure 1) measurements are reliable. This is the case up to the point of at least 14% electronic dead time from high rates of particles, which triggers COSTEP to switch into its designated low geometric factor mode. In most cases, this mode triggers by reaching the threshold value in the front detector of COSTEP (periods shaded yellow in Figure 1), which is susceptible to particles even below its nominal energy threshold of 4.3 MeV for ions. The COSTEP proton intensities are accurate throughout the onset and presumably well into (orange shading) periods of large dead time. COSTEP lower-energy proton data suffer from limited statistics during high electron-to-proton ratio periods, as discussed in Appendix A, but the times of proton onset can be derived quite accurately. This is illustrated in the velocity dispersion signature seen in the proton spectrogram of Figure 1.

[28] A technique has been introduced in Appendix A for comparison between channels from different detectors, here applied to GOES 8/SEM differential flux channels. The COSTEP data offer a choice of (arbitrary) combinations from the PHA-based COSTEP spectrogram data of narrow energy bands (from recorded energy losses) for comparison and thus provide a new tool for cross calibration. Despite the usual limitations in telemetry it should be regarded as a priority for new energetic particle detectors on to-be-developed space missions that, wherever the

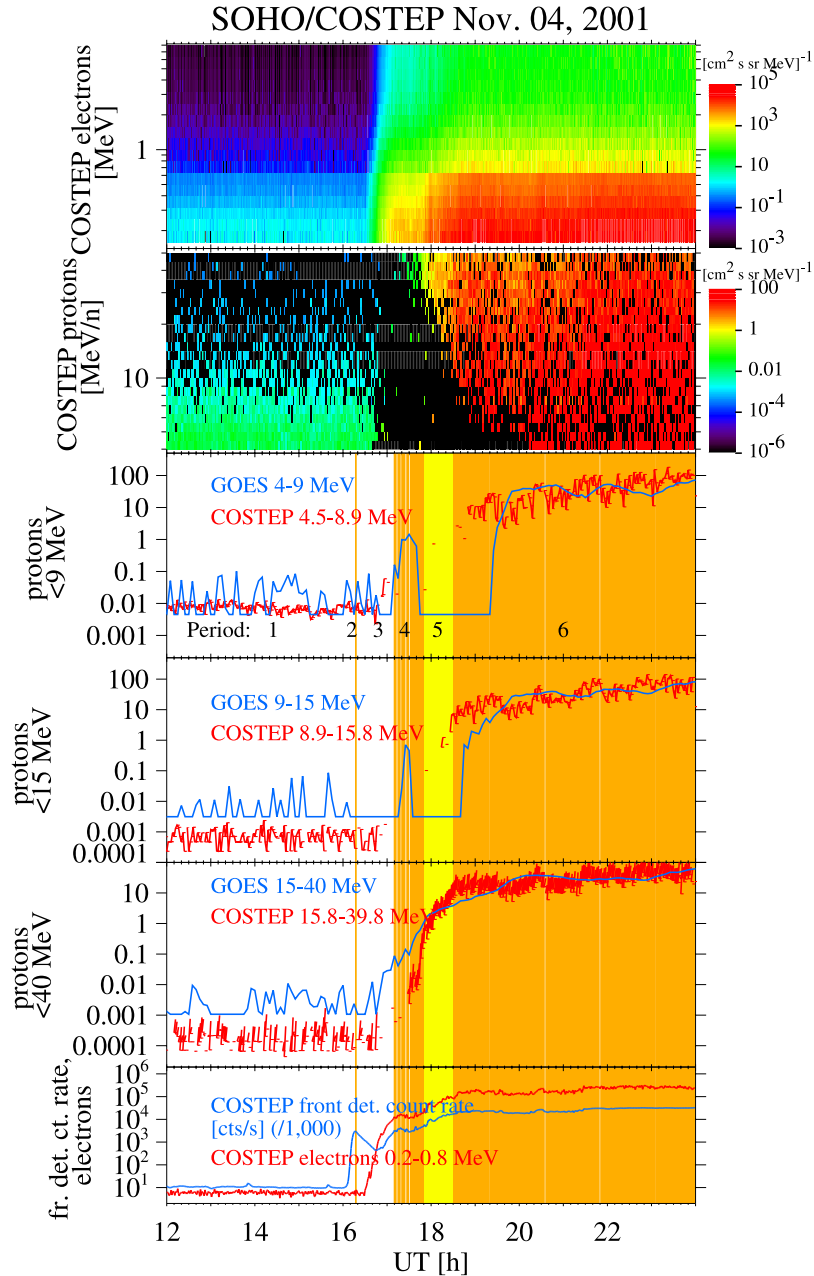


Figure 1. Top two plots show SOHO/COSTEP particle intensities for electrons and protons in the energy-time plane. The three middle plots show intensity-time profiles ($\text{cm}^2 \text{ s sr MeV}^{-1}$) for corrected GOES 8/SEM proton channels and for COSTEP protons with similar energy intervals. The bottom plot compares the COSTEP front detector count rate (blue) with the lowest-energy electron channel (red) intensity in ($\text{cm}^2 \text{ s sr MeV}^{-1}$). Shading in the bottom four plots indicates the state of the COSTEP instrument. The levels yellow (y) and orange (o) are explained in detail in the text.

scientific need for accurate particle event timing or cross calibration with other spacecraft might arise, they provide sufficient quantities of PHA-equivalent data products with their telemetry.

[29] As a result of the detailed comparison it has been shown that all low-energy GOES 8/SEM differential proton channels have problems throughout the SEP onset period with (1) electron and relativistic ion contamination

and (2) temporary overcorrection of lower-energy proton channels. Comparison with COSTEP helps to quantify these problems. Generally, the onset times cannot be derived accurately from <84 MeV differential proton channels of GOES 8/SEM. Note that error bars occur here that are as large as 90 min. Similarly, the onset differential intensities contain systematic errors. Despite warnings of the GOES team, differential proton data from GOES 8/SEM are in widespread use.

[30] However, late phases of SEPs, when highest proton intensities occur, presumably are covered accurately with GOES 8/SEM data. It is here, where COSTEP, an instrument devoted to measure small and intermediate SPEs with good statistics, has problems, in particular for the events with highest intensities.

[31] All periods of level orange, which exclude all phases of electronic pileup for COSTEP, have been excluded from statistical treatment. As a more reliable data set for deka-MeV protons currently is not available, we utilize COSTEP data only for the study of onset warnings.

[32] A hybrid data set of these two detectors would be desirable and would ease the current limitations of the use of the two separate proton data. This would, however, require further investigation into multiple scenarios between COSTEP and SEM that is beyond the scope of this report.

4. Relativistic Electrons and 30–50 MeV Proton Onsets

[33] The basis for this statistical and superposed epoch study is the GOES proton event list as published by NOAA. This list contains all major solar particle events, but also smaller and intermediate events. The only criterion is that at one point in time the >10 MeV protons exceed 10 proton flux units (protons exceeding 10 MeV $(\text{cm}^2 \text{sr s})^{-1}$, pfu). For simplicity, only full years of overlap between GOES 8 and SOHO energetic particle observations will be used here for the comparison, which include the years 1996 through 2002.

[34] Note that a new, more focused event list for human exploration activities should in the future provide lower limits of flux values in pfu above the more relevant threshold energy value of 30 MeV. Furthermore, interplanetary shocks often accelerate ions beyond 10 MeV in large numbers. However, their spectra are relatively soft and only few events can be detected beyond 30 MeV. The pfu maximum flux numbers therefore often contain large contributions originating from particles that do not harm human explorers. This fraction of the flux could be excluded with a threshold at 30 MeV (measured in, e.g., “human pfu” or “hpfu”).

[35] With the typical power law distribution for solar particle event maximum fluxes, a large fraction of the entries in this list are at the lower end of the spectrum just above the cutoff flux level of 10 pfu. Presumably, an even higher number of events will be situated just below the 10 pfu threshold. It would therefore be inaccurate to

claim that all GOES list entries as “major” events and all nonentries as “minor” events.

[36] The COSTEP data are complete over wide parts of this period, with the exception of two periods deemed SOHO “vacation” in 1998 and 1999. These periods are related to the sudden loss and subsequent recovery and reprogramming of the SOHO spacecraft. The common event list therefore contains 65 entries, as shown in Table 1a. The columns of Table 1a contain the following information.

[37] 1. “Event” identifies the event number in temporal succession.

[38] 2. “Date” provides the year and date (month and day) and the day of year of the onset of the solar particle event (in parentheses). Note that this date may deviate from the original GOES list by up to 2 days. The list identifies times when the >10 MeV proton flux exceeds 10 pfu, which can be delayed by days over the actual onset of the solar particle event.

[39] 3. “Time of Electron Onset” identifies the onsets of the 0.3–1.2 MeV solar energetic electrons, as measured by COSTEP. The onsets, where provided, are always associated with the upcoming proton event. Not all proton events on the GOES list are associated with prompt enhancements in solar energetic electrons fluxes. However, these types of events, as discussed elsewhere in this section, can be forecast with different methods.

[40] 4. “Protons, pfu” shows the fluxes of GOES 8 > 10 MeV protons in proton flux units $(\text{cm}^2 \text{sr s})^{-1}$ as published in the GOES list.

[41] 5. “Level e/p” identifies whether the COSTEP instrument experiences significant periods of low geometric factor mode (y = yellow) or dead time (o = orange) for onset parameter determination. It is provided whenever during a given onset time bracket the fraction of level yellow or orange exceeds 10% in time. As the rise phases of electrons and protons occur during distinct time intervals, the first value is determined for the electron onset, the latter for the proton onset.

[42] 6. “Flare Location” provides information on the flares that are most likely associated with the particle events.

[43] 7. “Connection Distance” provides the absolute value of the assumed connection distance of the observers’ magnetic foot point from the flare longitude on the Sun. Neither the flare nor the observers’ latitude have been taken into account.

[44] 8. “Nature of the event” information on the nature of the event, including (1) whether pre-event background significantly interfered with the observations (bg), (2) whether the event was irregular (irr), i.e., associated with a shock structure sweeping over the observer, (3) whether the onset of ACE/EPAM electrons indicated scatter-free transport from the Sun [Haggerty *et al.*, 2003] (scf), or (4) whether it was a ^3He -rich event according to the event list by Mason *et al.* [2004] (M).

Table 1a. GOES 8 > 10 pfu Particle Event List for 1996–2002, With Exception of Events During the SOHO Vacation in 1998 and 1999

| Event | Date | Time of Electron Onset | Protons, pfu | Level e/p | Flare Location | Connection Distance, deg | Nature of the Event |
|-------|-------------------------------|------------------------|--------------|-----------|---------------------|--------------------------|---------------------|
| 1 | 1997/11/04 (308) | 06:14 | 72 | -/- | S14W33 | 38 | scf |
| 2 | 1997/11/06 (310) | 12:14 | 490 | -/y | S18W63 | 3 | |
| 3 | 1998/04/20 (110) | 10:29 | 1700 | -/- | S43W90 | 30+ | |
| 4 | 1998/05/02 (122) | 13:45 | 150 | -/y | S15W15 | 23 | |
| 5 | 1998/05/06 (126) | 08:08 | 210 | o/o | S11W65 | 16 | scf, M |
| 6 | 1998/11/08 (312) | - | 11 | - | - | - | irr |
| 7 | 1998/11/14 (318) | 05:29 | 310 | -/- | N28W90 | 30+ | |
| 8 | 1999/04/24 (114) | 13:36 | 32 | -/- | NWlimb | 37+ | |
| 9 | 1999/05/03 (123) | 13:44 | 14 | -/- | N15E32 | 79 | |
| 10 | 1999/06/01 (152) | 19:18 | 48 | -/- | - | - | |
| 11 | 1999/06/04 (155) | 07:17 | 64 | -/o | N17W69 | 16 | scf |
| 12 | 2000/02/18 (049) | 09:30 | 13 | -/- | S16W78 ^a | 17 | scf |
| 13 | 2000/04/04 (095) | 15:23 | 55 | -/- | N16W66 | 6 | scf |
| 14 | 2000/06/06 (158) ^a | 16:42 | 84 | -/- | N20E18 | 69 | bg |
| 15 | 2000/06/10 (162) | 17:06 | 46 | -/- | N22W38 | ~7 | scf |
| 16 | 2000/07/14 (196) | 10:35 | 24000 | y/o | N22W07 | 30 | |
| 17 | 2000/07/22 (204) | 11:51 | 17 | -/- | N14W56 | 2 | bg, scf |
| 18 | 2000/07/28 (210) | - | 18 | - | - | - | irr |
| 19 | 2000/08/11 (224) | - | 17 | - | - | - | irr |
| 20 | 2000/09/12 (256) | 12:23 | 320 | -/- | S17W09 | 53 | |
| 21 | 2000/10/16 (290) | 07:32 | 15 | -/- | N04W90 | 51+ | |
| 22 | 2000/10/25 (299) | 10:29 | 15 | -/- | N00W90 | 33+ | |
| 23 | 2000/11/08 (313) | 22:57 | 14800 | -/o | N05W78 ^b | 28 | |
| 24 | 2000/11/24 (329) | 05:20 | 940 | -/- | N20W05 | 59 | |
| 25 | 2001/01/28 (028) | 16:17 | 49 | -/- | S04W59 | 14 | |
| 26 | 2001/03/29 (088) | 10:12 | 35 | y/- | N14W12 | 30 | |
| 27 | 2001/04/02 (092) | - | 1110 | - | N18W82 | - | bg (scf) |
| 28 | 2001/04/09 (099) | - | 355 | - | S23W09 | - | bg |
| 29 | 2001/04/15 (105) | 14:01 | 951 | y/y | S20W85 | 41 | |
| 30 | 2001/04/18 (108) | 02:33 | 321 | -/- | S20W90 | 44+ | bg |
| 31 | 2001/04/28 (118) | - | 57 | - | N17W31 | - | irr |
| 32 | 2001/05/07 (127) | 12:14 | 30 | -/- | NWlimb | 34+ | |
| 33 | 2001/06/15 (166) | 15:46 | 26 | -/- | Wlimb | 22+ | scf |
| 34 | 2001/08/10 (222) | - | 17 | - | - | - | |
| 35 | 2001/08/16 (228) | 00:17 | 493 | -/o | - | - | |
| 36 | 2001/09/15 (258) | 11:48 | 11 | -/- | S21W49 | 8 | |
| 37 | 2001/09/24 (267) | 10:48 | 12900 | y/- | S16E23 | 74 | scf |
| 38 | 2001/10/01 (274) | - | 2360 | - | S22W91 | - | bg |
| 39 | 2001/10/19 (292) | 17:00 | 11 | -/- | N15W29 | 40 | |
| 40 | 2001/10/22 (295) | 15:24 | 24 | -/- | S18E16 | 59 | |
| 41 | 2001/11/04 (308) | 16:29 | 31700 | -/o | N06W18 | 49 | scf |
| 42 | 2001/11/17 (321) | 05:48 | 34 | -/- | S13E42 | 96 | |
| 43 | 2001/11/22 (326) | - | 18900 | - | S15W34 | - | dg |
| 44 | 2001/12/26 (360) | 05:28 | 779 | -/y | N08W54 | 7 | |
| 45 | 2001/12/29 (363) | - | 76 | - | S26E90 | - | bg |
| 46 | 2001/12/30 (364) | - | 108 | - | - | - | irr |
| 47 | 2002/01/10 (010) | - | 91 | - | Elimb | - | |
| 48 | 2002/01/14 (014) | 08:38 | 14 | -/- | Wlimb | - | |
| 49 | 2002/02/20 (051) | 06:14 | 13 | -/y | N12W72 | 18 | scf, M |
| 50 | 2002/03/15 (074) ^a | 23:31 | 13 | -/- | S08W03 | 66 | |
| 51 | 2002/03/18 (077) | - | 53 | - | - | - | irr |

Table 1. (continued)

| Event | Date | Time of Electron Onset | Protons, pfu | Level e/p | Flare Location | Connection Distance, deg | Nature of the Event |
|-------|-------------------------------|------------------------|--------------|-----------|----------------|--------------------------|---------------------|
| 52 | 2002/03/20 (079) | - | 19 | - | S09W46 | - | irr |
| 53 | 2002/03/22 (081) | 11:06 | 16 | -/- | Wlimb | 39+ | scf |
| 54 | 2002/04/17 (107) | 08:31 | 24 | -/y | S14W34 | 33 | |
| 55 | 2002/04/21 (111) | 01:32 | 2520 | y/o | S14W84 | 47 | scf |
| 56 | 2002/05/22 (142) | 00:16 | 820 | -/- | - ^c | - | |
| 57 | 2002/07/07 (188) | 11:46 | 22 | -/- | Wlimb | 46+ | |
| 58 | 2002/07/15 (196) ^a | 22:53 | 234 | -/- | N19W01 | 67 | |
| 59 | 2002/07/19 (200) | - | 13 | - | - | - | irr |
| 60 | 2002/07/22 (203) | - | 28 | - | SElimb | - | bg |
| 61 | 2002/08/14 (226) | 01:55 | 26 | -/y | N09W54 | 1 | scf, M |
| 62 | 2002/08/22 (234) | 02:05 | 36 | -/- | S07W62 | 7 | |
| 63 | 2002/08/24 (236) | 01:14 | 317 | y/y | S08W90 | 31+ | scf |
| 64 | 2002/09/06 (249) | - | 208 | - | N09E28 | 78 | irr |
| 65 | 2002/11/09 (313) | 13:38 | 404 | -/- | S12W29 | 34 | |

^aDates adjusted to reflect particle event onset and flare date.

^bAverage values for longitude and latitude.

^cFalse flare identification in NOAA list according to COSTEP electron onset.

[45] A second event list has been added for comparison. This list originally contains 39 large so-called “impulsive” events as identified by *Reames and Ng* [2004] based on heavy ion ratios and fluxes, whereas Table 1a predominantly contains large, so-called “gradual” events. In the current paradigm, “impulsive” events are thought to be related to flare acceleration processes, and “gradual” events related to shocks of CMEs (see below for discussion). Table 1b shows a subset of the events identified by Reames and Ng for which sufficient information is available that allows a comparison with the events from the GOES 8/SEM list. Entry categories for Table 1b are a subset of those used for Table 1a, with one exception:

the second column of Table 1b identifies events with numbers from the Reames and Ng list.

4.1. Connectivity and Onset Slopes of the Intensity-Time Profiles

[46] From Table 1a, a total of 48 events have been identified as SEP events. Thirty-three events of this list are sufficiently complete in data coverage and are associated with flares of well-known location on the Sun, in particular with relative longitudes (E and W) less than 90°. All 48 events enter the statistical study of solar particle event onsets, with the exception of seven level orange events. Thirty-three events enter the study of connection longitude dependency, of which one event for electrons

Table 1b. List of Large “Impulsive” Particle Events Selected From *Reames and Ng* [2004] With Sufficient Information to Enter Comparisons With GOES List Events

| Event | <i>Reames and Ng</i> [2004] Event | Date | Time of Electron Onset | Flare Location | Connection Distance, deg |
|-------|-----------------------------------|------------------|------------------------|---------------------|--------------------------|
| 1 | 11 | 1999/02/20 (051) | 04:07 | S21W63 | 12 |
| 2 | 12 | 1999/02/20 (051) | 15:20 | S17W71 | 14 |
| 3 | 13 | 1999/06/18 (169) | 14:41 | N26W53 | 7 |
| 4 | 17 | 1999/12/27 (361) | 02:11 | N24W36 | 22 |
| 5 | 18 | 2000/03/07 (067) | 12:39 | S12W71 ^a | 20 |
| 6 | 20 | 2000/05/01 (122) | 10:24 | N21W51 ^b | 1 |
| 7 | 21 | 2000/05/04 (125) | 11:14 | S25W82 ^a | 33 |
| 8 | 23 | 2000/05/24 (145) | 21:13 | N22W43 | 6 |
| 9 | 28 | 2001/04/14 (104) | 17:50 | S16W71 | 37 |
| 10 | 31 | 2002/04/14 (104) | 22:35 | N18W74 | 17 |
| 11 | 32 | 2002/04/15 (105) | 02:57 | N19W79 | 19 |
| 12 | 35 | 2002/08/18 (270) | 21:30 | S12W19 | 20 |
| 13 | 36 | 2002/08/19 (271) | 10:44 | S12W25 | 19 |
| 14 | 37 | 2002/08/19 (271) | 21:08 | S11W33 | 13 |
| 15 | 38 | 2002/08/20 (272) | 08:30 | S10W38 | 8 |
| 16 | 39 | 2002/09/27 (310) | 01:36 | - | - |

^aFlare location from H alpha observations.

^bFlare location from SOHO/EIT EUV brightening.

and six for protons had to be excluded because of level orange.

[47] It has long been recognized that the magnetic connection geometry between the solar event and the observer in the heliosphere plays a critical role in the general morphology of the particle event [Cane *et al.*, 1988; Reames *et al.*, 1996]. These authors show case studies of overall intensity-time profiles for specific events that express a dependency in appearance of the magnetic connection geometry. The authors argue that CME shocks propagating radially outward from the Sun are ultimately responsible for the appearance of the proton intensity as the magnetic connection conditions to the observer at 1 AU change and sweep over the nose or other parts of the shock front.

[48] As a brief background, the heliospheric magnetic field expands radially from the Sun, as it is frozen in the solar wind. Solar rotation is responsible for the magnetic field to be twisted into Archimedean spiral geometry, thereby retaining the magnetic connection with its origin in the solar corona. This pattern has been predicted by Parker [1958] and confirmed by observations of the magnetic sector structure, i.e., time periods of inward or outward pointing magnetic field, in interplanetary space [Ness, 1968]. Accurate determination of solar source longitude and latitude of solar wind parcels and their embedded field lines [e.g., Liewer *et al.*, 2002; Posner *et al.*, 2001] continues to be a challenge for modelers [e.g., Schatten *et al.*, 1969; Wang and Sheeley, 1990; Linker *et al.*, 1999]. For our purposes, ballistic mapping in longitude suffices, as it is the intention to explore the possible existence of a statistical relationship between the particle event and its expansion on the field lines we observe. For each individual event, the solar wind speed measured by Wind/SWE at the time of onset is used. Ballistic mapping assumes radial, constant speed expansion of the solar wind from the Sun. The time derived for solar wind expansion to 1 AU is taken to derive the angle of rotation for the Sun in order to determine the W longitude of the corona that released the solar wind parcel near the central meridian. As connection distance (in longitude) we assume the absolute value of the angular distance of flare location longitude and magnetic connection longitude. Note that the connection distance does not take into account the magnetic latitude of flare or observer.

4.2. Characterizing Initial Increase in Particle Intensities With Statistical and Superposed Epoch Techniques

[49] The emphasis of this study is on the time of the onset of relativistic electrons. Typically, the intensity rise of relativistic electrons is rapid, as shown in Figure 1, following in nearly all cases an exponential increase with time. The observations show, as illustrated in Figure 2, that exponentials (straight-line fits in a semilog diagram) to the steepest part of the rise characterize quite well the

nature of the event. A single rise parameter is gained from this fitting procedure. Other, more detailed fits to the onsets of particle events exist, but simple exponential fits to the onset profiles are adequate for our purposes.

[50] Although the onset profile follows an exponential increase initially, at some point the intensity increase necessarily flattens or breaks into a more gradual rise. Of interest here is only the steepest, near-exponential part of the onset. We apply three techniques (two only for protons because of statistical limitations) here side by side in order to show the independence of the rise parameter from human-set boundary conditions. Here is the recipe:

[51] 1. Method 1: Onset-to-break method. Best estimates for onset of event and subsequent break in intensity increase toward a plateau or more gradual increase (unless increase is longer than a maximum duration of 5 hours). The entire period in between these two times is used for straight line fit in order to derive increase parameter. Figure 2 shows fits to the data with this method in all electron and proton plots (blue lines).

[52] 2. Method 2: Center interval of onset-to-break method. After employing method 1, the subinterval in its center with exactly half the interval duration is selected. The increase parameter is derived from a straight line fit to this (shorter) time period. Fits from this method, also shown in Figure 2 (green lines), are void of problems stemming from a lack of exact definitions of onset and break times. On the other hand, the accuracy suffers, in particular for proton onsets, for events with rather low statistics, i.e., larger scatter of the 2-min averaged fluxes.

[53] 3. Method 3: Steepest 10-min increase method. Fixed 10-min interval straight line fits are performed. The largest increase parameter value is selected for any event. Problems occur (1) for short, fast rising electron onsets where steepest increase is much shorter than 10 min, such as the event on top of Figure 2, and (2) for slow-rising onsets where electron intensity fluctuations are on the order of or higher than the intensity increase from the particle event. As the proton intensity increase takes much longer than the electron increase, and the statistical fluctuations are too large for the given detector geometry, this method cannot successfully be employed for proton onsets.

[54] By employing all three methods for electrons and methods 1 and 2 for protons, we established the new parameters Φ_e and Φ_p for all solar energetic particle events of the list of Table 1a. This analysis uses in all methods linear regression algorithms applied to the logarithm of the time-intensity profile for 0.3–1.2 MeV electrons with highest (1 min) time resolution and for 31–50 MeV protons with 2-min accumulation time. The result gives one value for each method for electrons: $\Phi_e = d(\log_{10}(I_e(t = t_2)/I_e(t = t_1)))/dt$ in $(\text{min})^{-1}$ and for protons $\Phi_p = d(\log_{10}(I_p(t = t_2)/I_p(t = t_1)))/dt$.

[55] Table 2a contains full information on selected time periods and the parameters gained from the various methods for comparison:

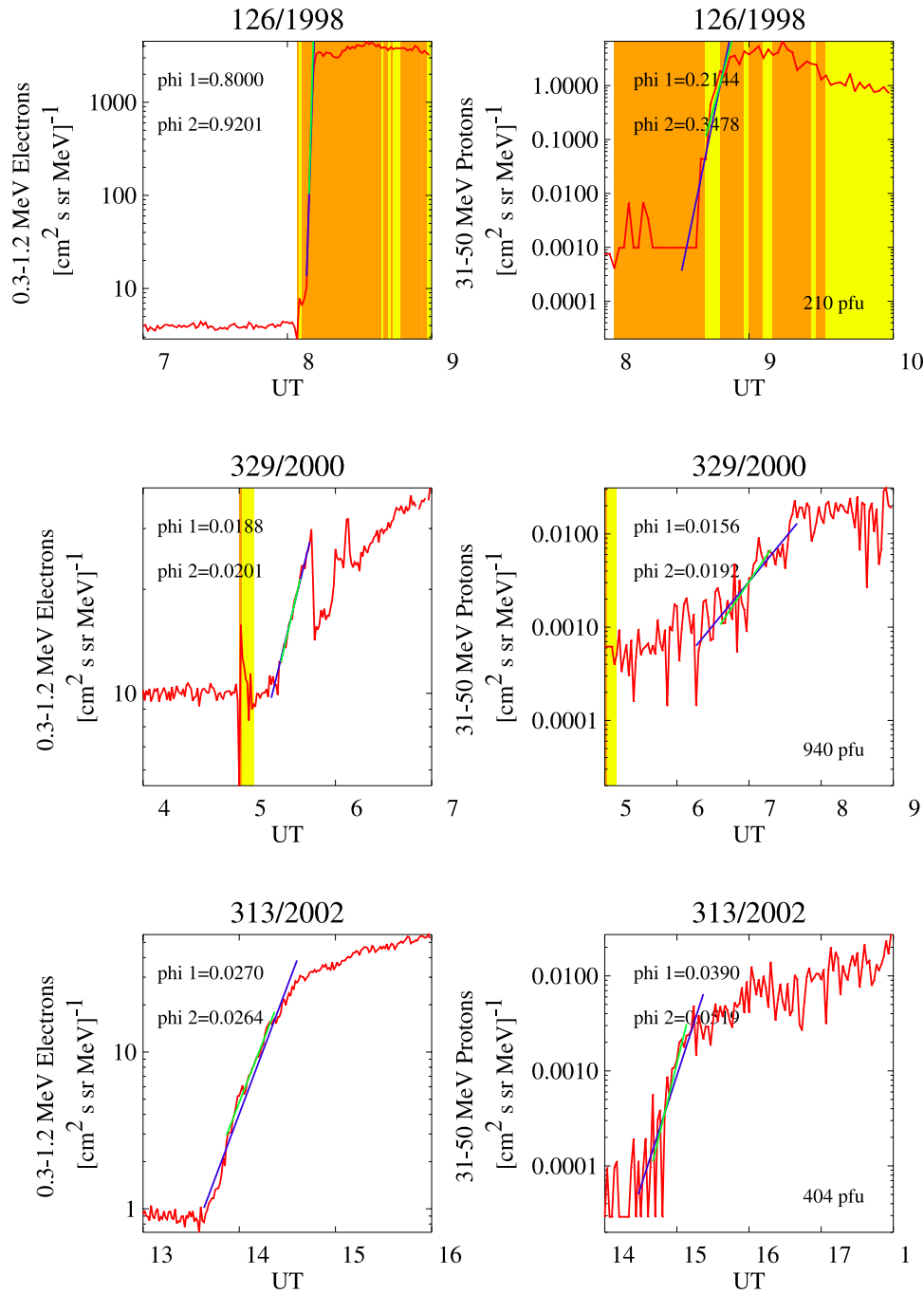


Figure 2. Three solar energetic particle events, numbers (top) 5, (middle) 24, and (bottom) 65 from the list in Tables 1 and 2, are shown with (left) electron and (right) proton time profiles. The plots show examples of exponential (straight line in semilog coordinates) fits of methods 1 (blue) and 2 (green) for electrons and protons. The straight lines extend over the periods of time of which the log of the intensity-time profile has been used for the linear regression fit. The background shading scheme has been adopted from Figure 1.

Table 2a. (continued)

| Event | Date | Method 1 Electron | | Method 1 Electron Onset End | Electron Onset Steepest 10-min Rise End | Φ_e | | | Proton | | Φ_p | |
|-------|-----------------------|----------------------|--------------------|-----------------------------------|---|----------|----------|--------------------|-------------------------|-----------------|----------|----------|
| | | Onset Start | End | | | Method 1 | Method 2 | Method 3 | Method 1 Onset Start | Method 1 End | Method 1 | Method 2 |
| 53 | 2002/081 | 11:06 | 11:26 | 11:12 | 0.0141 | 0.0083 | 0.0269 | 12:16 | 14:36 | 0.0047 | 0.0080 | |
| 54 | 2002/107 | 08:31 | 09:50 | 10:23 | 0.0225 | 0.0236 | 0.0979 | 10:00 | 12:30 | 0.0122 | 0.0125 | |
| 55 | 2002/111 | 01:32 | 01:52 | 01:40 | 0.1400 | 0.1217 | 0.2716 | 01:50 | 02:10 | 0.2921 | 0.2695 | |
| 56 | 2002/142 | 00:16 | 00:36 | 00:23 | 0.0368 | 0.0312 | 0.0530 | 05:20 | 07:40 | 0.0085 | 0.0045 | |
| 57 | 2002/188 | 11:46 | 12:08 | 11:54 | 0.0639 | 0.0455 | 0.1125 | 12:24 | 12:40 | 0.2209 | 0.0735 | |
| 58 | 2002/196 ^a | 22:53 | 01:00 ^b | 00:02 ^c | 0.0014 | 0.0002 | 0.0156 | 11:00 ^d | 15:00 ^e | 0.0071 | 0.0010 | |
| 59 | 2002/200 | - | - | - | - | - | - | - | - | - | - | |
| 60 | 2002/203 | - | - | - | - | - | - | - | - | - | - | |
| 61 | 2002/226 | 01:55 | 02:07 | 02:06 | 0.1013 | 0.0943 | 0.1079 | 02:30 | 02:54 | 0.0488 | 0.0826 | |
| 62 | 2002/234 | 02:05 | 02:32 | 02:25 | 0.0417 | 0.0545 | 0.0671 | 02:34 | 02:58 | 0.1398 | 0.2317 | |
| 63 | 2002/236 | 01:14 | 01:30 | 01:27 | 0.1433 | 0.1912 | 0.1803 | 01:48 | 02:10 | 0.0946 | 0.0974 | |
| 64 | 2002/249 | - | - | - | - | - | - | - | - | - | - | |
| 65 | 2002/313 | 13:38 | 14:36 | 13:56 | 0.0270 | 0.0264 | 0.0496 | 14:28 | 15:22 | 0.0390 | 0.0519 | |

^aDates adjusted to reflect particle event onset and flare date.

^bExtended window necessary (57% of method 1).

^cExtended window necessary (66% of method 1).

^dIntermittent data gaps 14:12–54.

^eIntermittent data gaps 17:12–32.

^fNegative proton onset parameter due to relatively stronger background fluctuations, treated as minimum positive value (0.0001) in statistical analysis of Φ_p .

^gNext day.

Table 2b. Increase Parameter List for Events of Table 1b

| Event | Date | Method 1 Electron Onset Start | Method 1 Electron Onset End | Φ_e Method 1 | Proton Method 1 Onset Start | Proton Method 1 End | Φ_p Method 1 |
|-------|----------|-------------------------------------|-----------------------------------|-------------------|-----------------------------------|---------------------------|-------------------|
| 1 | 1999/051 | 04:07 | 04:19 | 0.0827 | - | - | - |
| 2 | 1999/051 | 15:20 | 15:28 | 0.1107 | - | - | - |
| 3 | 1999/169 | 14:41 | 14:54 | 0.0335 | - | - | - |
| 4 | 1999/361 | 02:11 | 02:48 | 0.0168 | - | - | - |
| 5 | 2000/067 | 12:39 | 12:48 | 0.0697 | - | - | - |
| 6 | 2000/122 | 10:24 | 10:30 | 0.5213 | 10:48 | 11:02 | 0.1655 |
| 7 | 2000/125 | 11:14 | 11:20 | 0.1109 | 12:08 | 12:16 | 0.0434 |
| 8 | 2000/145 | 21:13 | 21:20 | 0.0375 | - | - | - |
| 9 | 2001/104 | 17:50 | 17:56 | 0.1100 | - | - | - |
| 10 | 2002/104 | 22:35 | 22:41 | 0.1128 | - | - | - |
| 11 | 2002/105 | 02:57 | 03:02 | 0.2909 | - | - | - |
| 12 | 2002/270 | 21:30 | 21:48 | 0.0426 | 22:20 | 22:40 | 0.0694 |
| 13 | 2002/271 | 10:44 | 10:48 | 0.1383 | - | - | - |
| 14 | 2002/271 | 21:08 | 21:15 | 0.1569 | - | - | - |
| 15 | 2002/272 | 08:30 | 08:42 | 0.0849 | 08:58 | 09:06 | 0.1048 |
| 16 | 2002/310 | 01:36 | 01:44 | 0.2328 | 02:16 | 02:22 | 0.4063 |

[56] 1. “Event” identifies the event number in temporal succession. The numbers are identical with Table 1.

[57] 2. “Date” provides the year and the day of year of the onset of the solar particle event, also corresponding to Table 1.

[58] 3. “Method 1 Electron Onset Start” identifies the beginning of the time period of onsets of the 0.3–1.2 MeV solar energetic electrons for determining the onset parameter with method 1.

[59] 4. “Method 1 Electron Onset End” marks the end of the time period of onsets of the 0.3–1.2 MeV solar energetic electrons for determining the onset parameter with method 1.

[60] 5. “Electron Onset Steepest 10-min Rise End” marks the end of a 10-min period for onset parameter determination according to method 3.

[61] 6. “ Φ_e Method 1” provides the onset parameters according to method 1.

[62] 7. “ Φ_e Method 2” provides the onset parameters according to method 2.

[63] 8. “ Φ_e Method 3” provides the onset parameters according to method 3.

[64] 9. “Proton Method 1 Onset Start” identifies the beginning of the time period of onsets of the 31–50 MeV solar energetic protons for determining the onset parameter with method 1.

[65] 10. “Proton Method 1 End” marks the end of the time period of onsets of the 31–50 MeV solar energetic protons for determining the onset parameter with method 1.

[66] 11. “ Φ_p Method 1” provides the onset parameters according to method 1.

[67] 12. “ Φ_p Method 2” provides the onset parameters according to method 2.

[68] Out of the “impulsive” event list in Table 1b, the increase parameters for electrons and protons have also been determined and entered into Table 2b. Because of

the relative weakness of these events, only method 1 determination of increase parameters has been conducted.

[69] For a thorough comparison, all increase parameters derived from three methods are present in Table 2a. In addition, Figure 2 provides three examples of the electron and proton onset fit procedures. The example on top is from the SEP event on day of year (DOY) 126, 1998. It shows the problems faced by an event onset that rapidly, within 4 min of electron onset, reaches critical flux level at 1 AU. The onset parameter is very high for electrons and protons.

[70] The second event, recorded on DOY 329, 2000, shows a slow intensity increase. It is regarded as the most problematic case, as one phase of the electron onset appears relatively steep, but the intensity suddenly drops resulting in another onset with much more moderate increase. Note that the Wind spacecraft encountered multiple sector boundary crossings between DOY 328 1700 UT and DOY 329 1200 UT. It is therefore likely that the electron onset has been interrupted by a local change in magnetic polarity or associated propagation conditions in the vicinity of the current sheet for SEPs at 1 AU. This question will be addressed in the next section.

[71] Solar flare X rays, as discussed more generally in Appendix A, play a role in this event. Note that, for a brief period of time, a problem arises for COSTEP electron observations. During the large flare preceding the event, a small numbers of X rays generate Compton electrons energetic enough to be measured in the two front SSDs and thus counted as solar electrons.

[72] The event at bottom of Figure 2 has been observed on DOY 313, 2002. With this event there have been the least problems of this set of three in determining the increase parameter. Both methods produce relatively

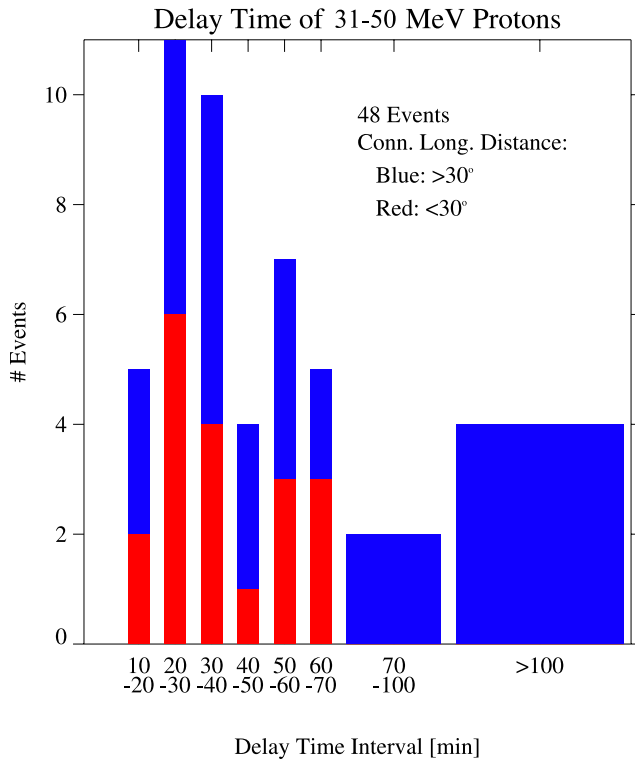


Figure 3. Histogram shows the distribution of 31–50 MeV proton onset delays over relativistic electrons. The diagram uses 48 SEP events from 1996–2002 with their observed delay times.

similar results for the intensity increase parameters across methods for electrons and protons.

4.3. Statistical Analysis of Onset Delays

[73] What insight does statistical treatment of onset delays of protons over relativistic electrons provide? All intensity increase parameters for SEP event protons and electrons from Table 1a, along with their respective time intervals, have been merged into Table 2a. The event numbers correspond to the list in Table 1a for easier comparison.

[74] One important statistical result from the onset fitting analysis is the average delay of the <50 MeV protons over relativistic electrons. The theoretical minimum value for the delay is 21.8 min. The average SEP onset time delay between e^- and p^+ as the times when the exponential fits cross the natural background (which varies from event to event) is 63.3 min, as determined from 48 solar particle events in this study. The minimum delay of only 13 min has been found in the 14 July (Bastille Day) event of 2000. The maximum delay is uncertain, but on the order of 10 hours in the event on 15 July (DOY 196) 2002. With the exception of event 55 (DOY 111, 2002, 18 min) all events with delays of less than 20 min are either extremely intense events, where level orange has been triggered by electrons (and/or preceding flares), or extremely weak,

where a marginal rise lasts for hours. In both cases the exact onset time delays carry uncertainties of likely more than 10 min. As the time resolution for protons is 2 min, and the upper energy limit is not a fixed value because of small effects from proton straggling, these results are not in contradiction to the assumption of simultaneous release of electrons and protons at the Sun.

[75] Figure 3 shows a histogram of <50 MeV proton onset delays for 48 SEPs of Table 1a. The distribution appears to have two peaks, although at the margin of statistical certainty. Presumed the peaks are real, the early peak is found at a delay near 20–30 min, whereas another shallow peak is observed at \sim 1 hour delay. Connection longitude information is also shown, with well-connected events with longitude distances between flare and observer of up to 30 degrees shown in the red fraction of the histogram. Well-connected events have proton delays of approximately up to 1 hour. On the other hand, not well connected events can also have relatively short proton delays.

[76] The mixing of short delay times with well and not-so-well connected events and the relatively common delay of up to 1 hour of well-connected events makes apparent that other factors besides connection distance might contribute. It seems likely, in particular with respect to event 24 (DOY 329, 2000, shown in the middle of Figure 2), that the relative magnetic polarities of the source and the observer in the heliosphere have influence on risetimes and onset delays. This unique event even reveals two rise constants for electrons, one fast and one slow, in connection with polarity reversals observed by the Wind spacecraft. It is likely that this effect also is responsible for the occurrence of two types of events, termed delayed and prompt. Presumably, prompt events are observed within the magnetic sector the particles are released into. Such findings have been previously reported from observations of Helios A and B [Kallenrode, 1993].

[77] Given the short timescale of the electron intensity increase and the relatively short average delay of protons (\sim 1 hour), in context with on average only 2–4 sector boundary crossings per (27-day) solar rotation period, this problem does not significantly limit the success rate of a forecasting method using the electron signal.

[78] The second effect potentially influencing the rise-times of (\sim 20 MeV) SEP ions might be related to CME speed, as found by Kahler [2005] for well connected (65° W to west limb) events with flare signatures in $H\alpha$, EUV or X rays. While the author claims support of his finding for a CME bow shock acceleration model, which is in conflict with the finding that fast CMEs without flare signatures do not produce conspicuous amounts of SEPs [Marqué et al., 2006], fast CMEs might rather rapidly open up magnetic connections between a flaring region and the observer with the effect of faster increase of particle intensities at 1 AU. This view would be consistent with the Kahler [2005] result that the CME speed effect works the same way in fast as in slow wind regimes, as determined by the in situ oxygen freeze-in temperatures. The relatively low corre-

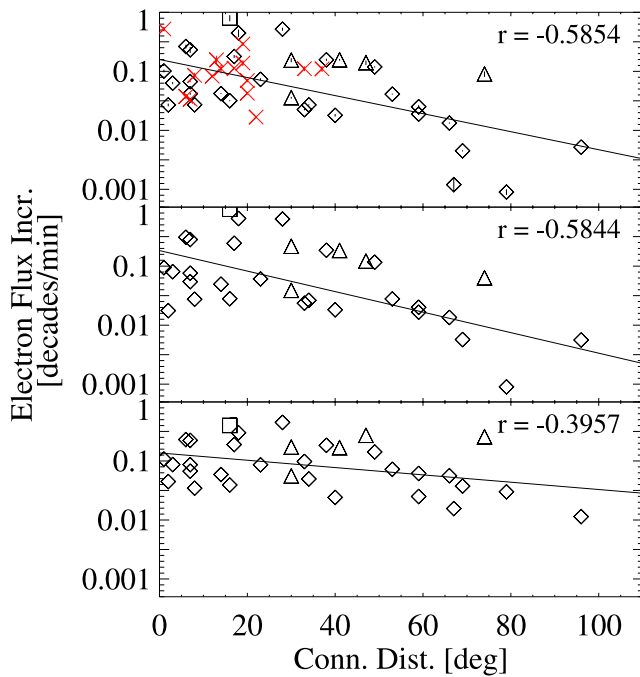


Figure 4. Plots display 0.3–1.2 MeV electron increase parameters over connection distance of the observers’ magnetic foot point to the flare location. Parameters have been derived via the three methods outlined in the caption of Table 2a: (top) method 1, (middle) method 2, and (bottom) method 3. The triangles indicate events with COSTEP in low geometric factor mode that have relatively higher statistical uncertainties than events indicated by diamonds. The correlation coefficient r is provided in each plot. Red symbols in the top plot indicate “impulsive” events from Table 2b for comparison.

lation coefficient (0.48 as compared to 0.66 for the longitude separation effect) and lack of correlation outside the stated source region range suggests that particle transport effects outweigh the CME speed effect.

4.4. Statistical Correlations Between Rise Parameters and Magnetic Connection

[79] What is the statistical relationship of inverse e -folding time with the connection distance of the observer’s magnetic foot point to the flare site, and how does the connection parameter affect onsets for relativistic electrons and >30 MeV protons? Black symbols in Figure 4 reflect the rise parameters of the initial electron intensity increase for 32 (“gradual”) solar particle events (one event removed because of COSTEP level orange) over connection distance for all three methods. We find a fast rise for well-connected events and slow intensity increases for events with a large magnetic connection distance.

[80] The correlation between the connection distance and Φ_e is expressed in the correlation coefficient $r =$

-0.5795 for method 1, $r = -0.5769$ for method 2 and $r = -0.3777$ for method 3. For this value of r , the likelihood of being exceeded by a pair of unrelated parameters of length 32 is less than 0.03%, 0.04%, and 2.76%, respectively. All three methods give statistically significant results, the first two methods even extremely statistically significant correlations. The effects pointed out in the description of method 3 limit the bandwidth of values for the electron increase parameter that in return leads to the lower correlation coefficient.

[81] The top plot also contains red symbols for events from Table 2b. For the given representation, the distribution of these “impulsive” events matches the distribution of large (“gradual”) events. The span of longitudes covered by these events reaches 37° distance from the flare longitude. Often, the full cone angle of injection of particles into the heliosphere in “impulsive” events is reported in the literature as 30° . This has to be corrected up to at least 74° for electrons.

[82] As a next step, we look into whether the influence of connection distance to electron increase is also observed in the initial increase of energetic protons as expressed in Φ_p . For this, methods 1 and 2 have been used with proton onsets for the above events of Tables 2a and 2b (method 1 only) in the same way as for relativistic electrons.

[83] Figure 5, which displays with black symbols the proton increase coefficient Φ_p of Table 2a (“gradual”) events over angular magnetic connection distance for

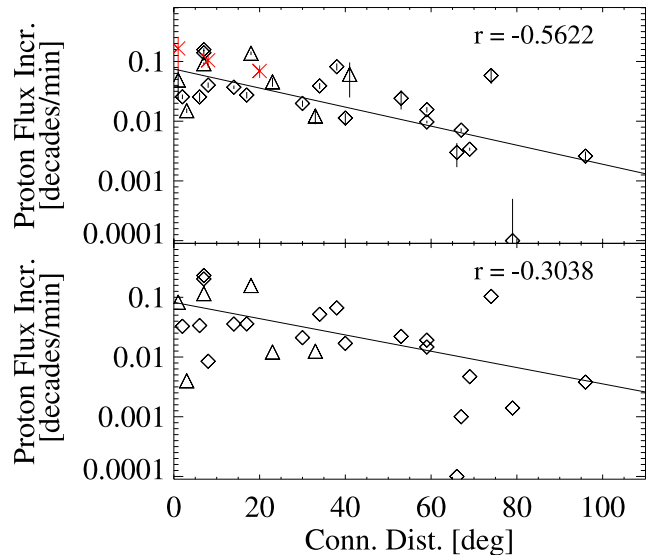


Figure 5. Plots show increase parameters for solar energetic particle event onsets of 31–50 MeV protons, derived with methods 1 and 2 (protons provide too low statistics for method 3) as outlined in the text, over connection distance in longitude of the observers’ magnetic foot point to the flare. The black symbols have the same meaning as in Figure 2. Red symbols in the top plot indicate “impulsive” events of Table 2b for comparison.

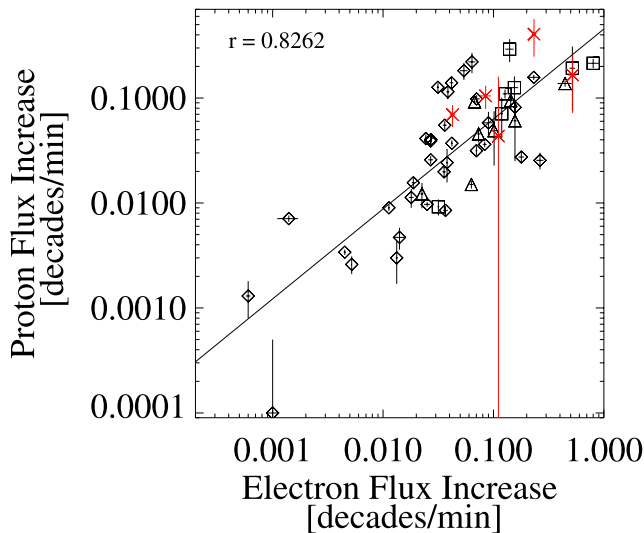


Figure 6. Plot shows correlation of increase parameters of protons and relativistic electrons for the onsets of solar energetic particle events from the GOES list (black) and from a list of “impulsive” events (red) observed in 1996–2002. Black symbols indicate the state of COSTEP during the rise in electrons and protons, with triangles indicating low geometric factor mode. The squares indicate high flux levels during at least one of the onsets. These and the “impulsive” events have not been used for the fit.

methods 1 and 2, shows that we indeed observe similar effects for protons. Protons show the same characteristic behavior of a steep, near-logarithmic increase immediately after the onset. The significance of a dependency of Φ_p on the connection distance is high for a correlation coefficient of $r = -0.5622$ for method 1 and -0.3038 for method 2. Only less than 0.15% or 11.6% of unrelated parameters of the length 27 (six events removed because of COSTEP level orange) and 26 (one additional event removed because of intermittent data gaps), respectively, exceed the values of the analyzed parameters. The results are very statistically significant and just outside statistical significance for methods 1 and 2, respectively. The general result is not surprising, as other authors have already found a connection linking the proton intensity profile with magnetic connection distance [Van Hollebeke *et al.*, 1975].

[84] In red symbols, the distribution of the few “impulsive” proton events has been added. The number of events is so limited because of the high threshold value of 30 MeV, which is rarely reached by these weaker events. Statistical scatter of three events has a large error bar. All events are located close to the regression line from “gradual” events. There is no indication of a systematic deviation of the “impulsive” events from the general distribution of large, “gradual” events.

[85] In fact, the similarity in the behavior of electrons and protons for all types of events motivates to test the

potential of the electron increase parameter for predicting the increase coefficient, i.e., the early time profile, of protons. Figure 6 provides us with the cross correlation of relativistic electron increase with energetic low-MeV proton increase. As here the knowledge of connection distance is not relevant, all 48 large (“gradual”) events have been considered for analysis. Removal of 6 events in which COSTEP observes the onset in level orange limits the total number available to 42. The relative increase coefficients for both particle types are highly correlated, $r = 0.8262$. Probabilistic analysis gives a negligible likelihood ($<1. \times 10^{-4}\%$) for a random distribution of 42 uncorrelated parameter pairs to exceed this value. Note that this correlation cannot be an instrument artifact, as both parameters are recorded at different times (see Table 2a) because of the much slower relative propagation of protons. Also, there is again no systematic difference between the distribution of the 42 “gradual” and five “impulsive” events (red symbols).

4.5. Superposed Epoch Analysis for Flare-Related Events 1996–2002

[86] By exploiting the potential of forecasting hazardous energetic proton arrival with relativistic electrons it is necessary to quantify the relationship of onset information with overall flux profiles, and in particular with the detailed time intensity profile right after the onset. As a first step, all 48 large SEP events with their respective time-intensity profiles have been combined into a set of three superposed epoch analyses, shown in Figure 7. Note that this method is rather crude and ignores systematic dependencies on source longitude [e.g., *Shea and Smart*, 1990]. However, as a first attempt, also longitude-independent studies such as that of *Townsend and Neal* [2006] using a Bayesian method provide important insight in SEP radiation forecasting.

[87] In this study, events enter the high- (red/orange), middle- (green) and low-level (blue) event categories of 16 events each according to their percentiles ordered by maximum fluxes given in the GOES list. The highest flux percentile has the widest span of maximum fluxes (300 to $\sim 30,000$ pfu), separated by a factor of 100. The midpercentile has a factor-of-10 span (30–300 pfu), and the lowest percentile only a factor-of-3 span (10–30 pfu) in maximum flux. There are onset 8-hour and main event 72-hour intervals shown. All COSTEP events have been reduced to the reliable data, meaning that all times with level orange, even for parts of events, have been excluded. The “coverage” plots give an indication as of what percentage of events contributed at any one time.

[88] For reasons discussed in section 3, electrons are provided by COSTEP only, and these are shown over the 8-hour interval alongside protons. The electron “drop-outs” originate from removal of the strongest event(s) in this group. In order to interpret the electron data, the low-intensity phases should be disregarded and instead an envelope of highest fluxes for electrons in each percentile

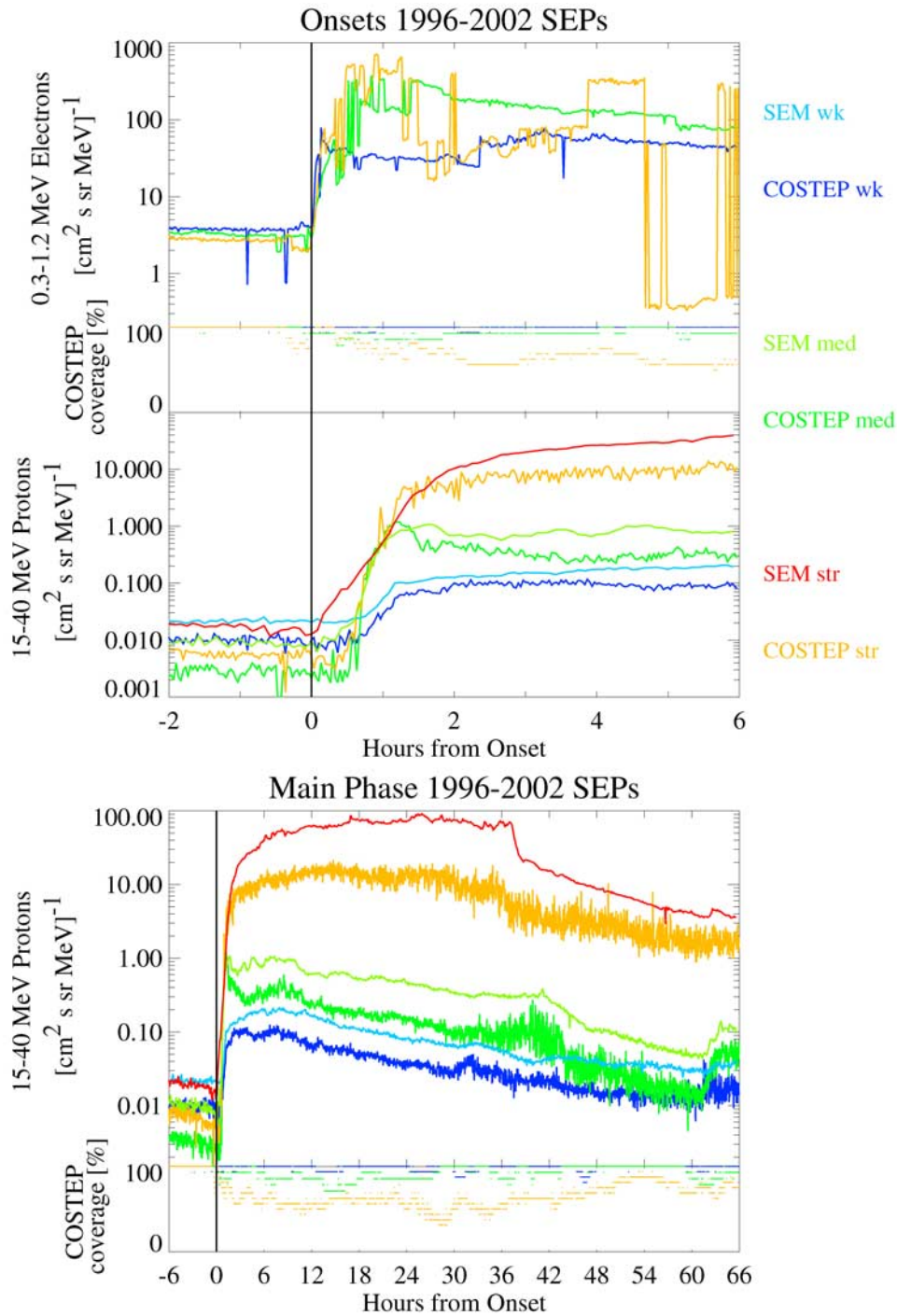


Figure 7. The 1996–2002 SEP events analyzed with the superposed epoch technique have been ordered in three groups representing the upper (str), medium (med), and lower (wk) third percentiles in GOES maximum proton flux. In each proton graph, COSTEP and SEM observations are shown; electrons are from COSTEP only. A vertical line at electron onset is the common time marker for each event. The resulting superposed epoch diagram displays 8 hours of 0.3–1.2 MeV electron and 8 and 72 hours of 15–40 MeV proton onsets with particle intensities averaged for these up to 16 events each. The two “coverage” graphs display the percentage of COSTEP in nonstate orange, as unreliably high fluxes had to be removed.

group combining the maxima considered. This envelope gives a more accurate impression of the average electron fluxes from these events.

[89] The superposed epoch diagrams for protons show the average particle event profiles for the three percentile ranges. In the strong event range, GOES 8/SEM (red) data are inaccurate at the onset, as discussed in section 3. Here, the combined COSTEP onsets (orange) are more physically plausible. Besides the onset problem, the combined data are generally at slightly higher intensities for SEM observations as compared to COSTEP, most noticeable in the highest percentile.

[90] The relevant findings of superposed epoch analysis are (1) relativistic electrons are always observed well in advance of the onset of protons and (2) the maximum electron intensities of the combined events are ordered in the same way as the maximum proton fluxes. In fact, intensities increment by significant factors from one percentile series to the next (lower-medium-upper) for both electrons (~ 80 , 300, >700 pfu/MeV for 0.3–1.2 MeV electrons) and protons (~ 0.1 , 1, and >10 pfu/MeV for 15–40 MeV protons).

[91] The relativistic electron precursor cautions on average more than 1 hour ahead of time the arrival of 15–40 MeV protons. Note that, on average, the most dramatic increase in proton intensity sets in with the above-specified delay after the warning interval, and lasts up to 30 min. Most of the increase is observed within approximately 2–3 hours after the electron warning with only marginal proton intensity increases for the strongest events beyond that time. There are long-term average (3-day) proton event profiles that presumably can be forecast with relativistic electrons onset data.

5. Solar Particle Event Forecasting Technique

[92] Section 4 has revealed (1) the similarity in the behavior of electrons and proton increase parameters and (2) correspondence of the ordering between electron and proton maximum intensities between several categories of events ordered in size by protons. It is therefore straightforward to attempt forecasting proton fluxes with relativistic electron onset observations. As a first attempt, 1-hour advance forecasting for the year 2003 has been undertaken with the sole aims at demonstrating (1) a low miss rate and (2) a low false alarm rate. The details are described in this section.

5.1. Forecasting Matrix

[93] As the forecasting potential for protons is limited in time for prompt events, necessarily the very first minutes of the electron onsets have to be used. Other, less prompt events with slower risetimes offer more extended electron observations to be used. There is a limit when it comes to events with extremely slow increase in protons, for which nowcasting is more useful than forecasting. Typically, these (badly connected) events are not as hazardous since

their maximum intensities are less likely to reach hazardous levels [Kunow *et al.*, 1991].

[94] The results from section 4 have also pointed out complications and limitations for forecasting. For example, statistical fluctuations cause variations in the electron rise parameter when fluxes are in the low-intensity regime. Therefore use of the rise parameter by itself can cause large numbers of false warnings. In order to limit false warnings, the additional positive correlation of early electron intensity with the upcoming solar proton intensity will be employed in order to provide a parameter for forecasting. The relatively smaller statistical fluctuations at higher electron fluxes effectively remove false warnings from small-scale fluctuations. Also, possible false warnings from well-connected, but overall weak solar particle events, often referred to as “impulsive” events, presumably are excluded. These presumptions have to be tested with actual data.

[95] The two electron parameters that have been shown as relevant for forecasting, flux and Φ_e , have been utilized in a phenomenological forecasting technique that we introduce here. The observations from 1996 to 2002 provide a substantial statistical sample for parameter pairs of Φ_e and flux. An algorithm has been developed that analyses all 1996–2002 COSTEP 0.3–1.2 MeV electron observations with a sliding 1-hour window. The algorithm searches every minute for the 5-min to 1-hour period, always ending in the most recent minute, that measures the highest positive electron rise parameter. A 5-min sample as the smallest permissible time interval is chosen because of the experience with method 3, requiring shorter intervals for the most fast-rising events. In the sample, method 3 uses linear regression in a fixed 10-min window for establishing the electron rise parameter. This critically limited the bandwidth at the high end, as electron increases of prompt SEP events often are shorter than 10 min.

[96] The second parameter utilized is the most recent electron intensity. With this method, the entire 6-year period provides on the order of 2 million 1-min pairs of parameters. All parameters fall into the respective boxes of the 13×18 forecasting matrix, which is shown in Figure 8. The entry that is provided from each parameter pair is the proton intensity measured 1 hour later, taking into account the on average 63 min delay of proton onset over electrons.

[97] Figure 8 has been color coded with the average of the upcoming proton intensities for each electron rise–electron flux pair combination. In this matrix, most entries fall into the boxes on the lower left, indicating low and near-constant electron intensity. The entries with significant increase parameters for electrons on the right have predominantly originated from short periods during solar particle event onsets of nearly all of Solar Cycle 23. Although quite a number of SEPs have been recorded, the statistical sample can be quite limited for certain matrix elements. This is particularly true for matrix elements representing the rare ground-level event combinations for intensity and Φ_e . It is therefore necessary to

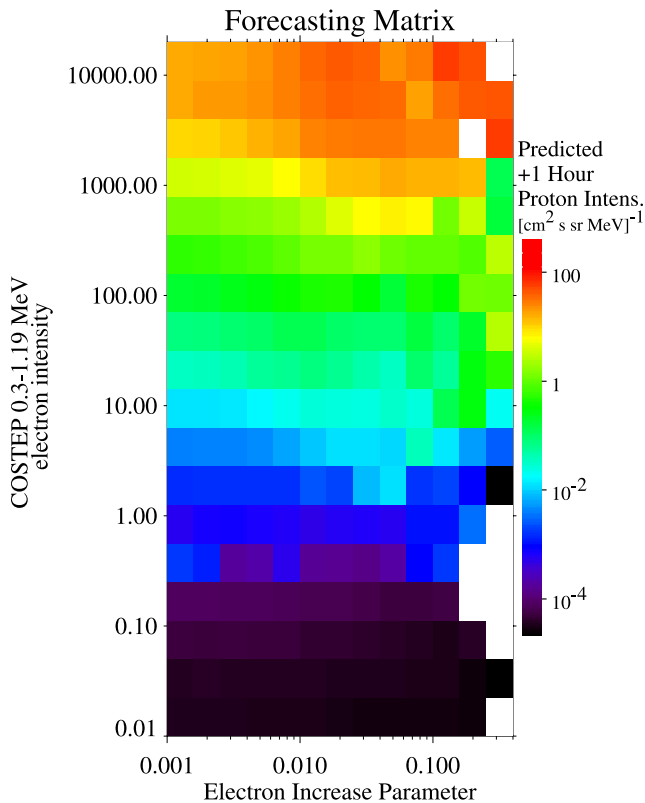


Figure 8. This color matrix provides a color code for the future proton intensity, 1 hour ahead of time, as predicted by relativistic electron measurements. The parameter space is given by the current maximum electron increase parameter, going back in time for at least 5 min, but up to 60 min, and the current relativistic electron intensity. The matrix is derived from the aggregate of all 1998–2002 relativistic electron observations and their corresponding 30–50 MeV proton intensities 1 hour later. The color shows the average for the proton intensity in each locus. Low statistics limit the extent of the matrix to the bottom and upper right.

continuously improve on the statistical accuracy of this matrix with additional statistics from more recent and upcoming data. An alternative is to look for a functional approximation of areas with good statistics that can be extrapolated in the undersampled region. Specifically for the most extreme events, this technique might be superior to the actual measurements (from COSTEP), as the reliability of in situ particle detection can suffer from electronic pileup.

[98] Within the matrix, a typical event progresses from the mainstream location upward and toward the right, when a particle event sets in. After that, it progresses minute by minute upward, and turning left as it reaches a plateau or follows the suggested \sin/h intensity-time profile referred to earlier. Although the progression has been

exploited here only in a limited way, forecasting from individual entries alone provides unprecedented results, as will be shown in the upcoming subsection.

5.2. Forecasting of Hazardous Ion Events in 2003

[99] Figure 9 (top) shows the sum of all minute-by-minute 1-hour advance 30–50 MeV proton flux predictions for the year 2003 (black) alongside the actual measurements (red). Note that the matrix utilizes only previously recorded data up to the end of 2002 in order to simulate a realistic situation. The COSTEP data for 2003 are near complete, but only the first 11 months of 2003 have been available for this study.

[100] As a filtering technique for the raw forecasts we make the (reasonable) assumption that 20 pfu (hpfu) defines a threat level for humans and/or technology in space. A dashed horizontal line indicates the “critical” intensity of $1 \text{ (cm}^2 \text{ s sr MeV)}^{-1}$ of 30–50 MeV protons, which is equivalent to ~ 20 pfu from the 30–50 MeV energy range alone.

[101] The second plot from top shows the ratio of forecast proton intensity relative to current intensity (f_c). The onsets of SEPs show series of high f_c when not preceded by elevated intensities. This parameter can be used as a tool for further filtering and is a good identifier for SPEs generally. At high intensity levels, such as through the Halloween event series to be discussed below, a potential filtering value needs to be adjusted to lower thresholds. No such filtering has been applied in this study.

[102] The actual warning time on the order of minutes to hours until onset of the protons event, or reaching the hazard level, cannot be resolved in the full-year view. Therefore the bottom two plots show increasingly expanded views of event time profiles during the Halloween storms in October and November 2003. The Halloween storms [Mewaldt *et al.*, 2005b] consist of a series of eight X class flares and tens of fast coronal mass ejections with their root cause in a large active region complex. Among them are X flares that entered the list of most extreme events ever observed. The associated energetic particle environment at 1 AU has also been at extreme levels and since observations have been used to calibrate spectra for the worst and life-threatening event within the last 500 years, the Carrington flare from 1859 [Stephens *et al.*, 2005].

[103] The comparison of 1-hour advance forecast of proton fluxes with the actual observations reveals a reasonable resemblance. Forecasts predict on average slightly higher fluxes than are observed, in particular for the declining phases of the latter Halloween solar events. The reason for this will have to be investigated. On the one hand, the 1996–2002 data flowing into the forecasting matrix might still be too limited to accurately predict considerably extreme space weather conditions. On the other hand, the technique presented here is intended to forecast the onset of events, not the decline. A second forecasting matrix, taking into account the maximum flux decrease (instead of the increase) encountered in the given

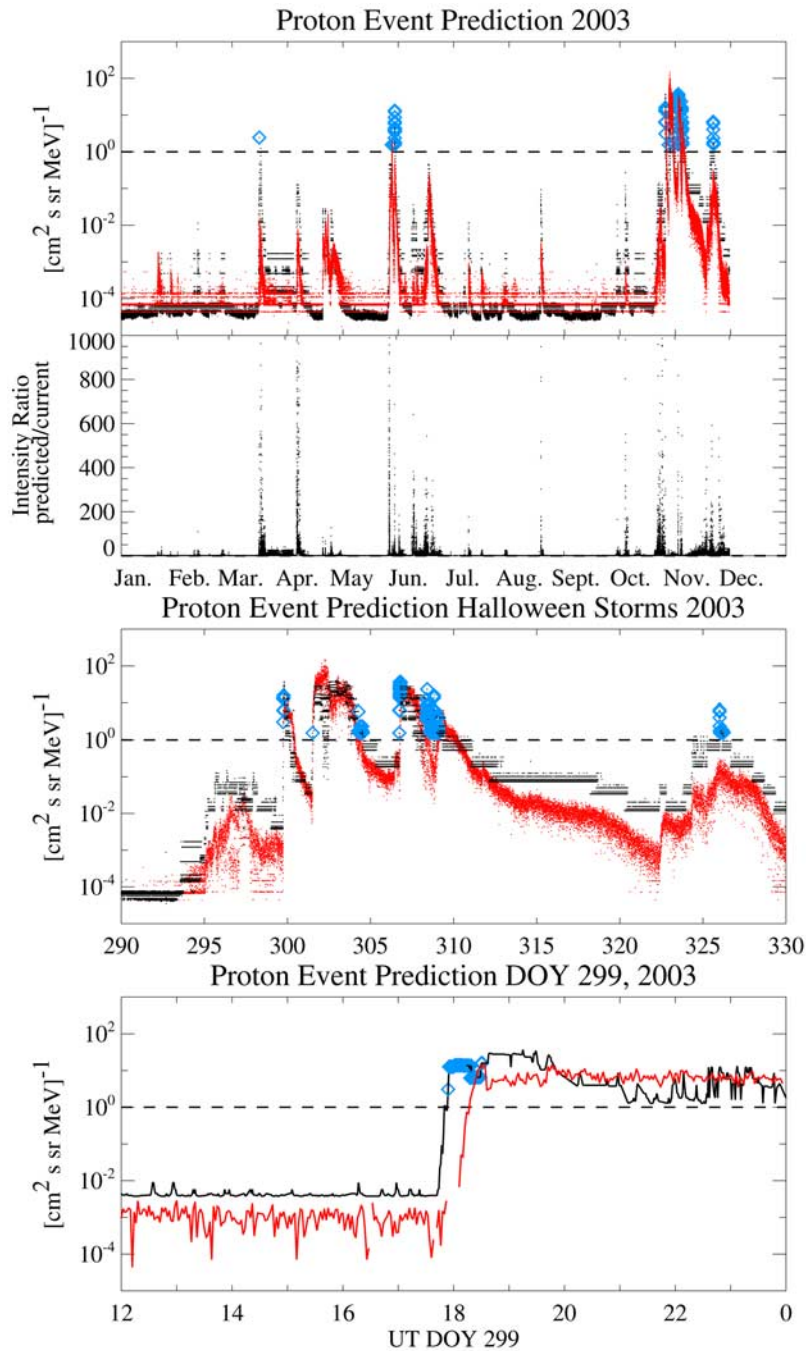


Figure 9. (top) Observed (red) and predicted (black) 30–50 MeV proton intensities are shown for the first 11 months of 2003. Blue diamonds indicate hazard warnings. The observations show 2-min averages. The 1-hour advance predictions, which are based on observations of 2003 relativistic electrons and the 1998–2002 matrix (Figure 8), have 1-min time resolution. (middle) Predictions for the October/November 2003 Halloween storms are shown. (bottom) Plot shows zoom into the onset of the individual particle event starting on DOY 299. Here one can resolve the advance warning of hazardous proton fluxes from relativistic electrons (black) compared to the observations (red).

Table 3. Warning Series Issued by the Introduced Forecasting Technique in 2003

| Warning Series | Date in 2003 | Warning Start, UT | Warning End, UT | Predicted Flux Range, ^a (cm ² s sr MeV) ⁻¹ | Observed Peak Flux, ^a (cm ² s sr MeV) ⁻¹ | Event Type | Advance Warning Time, min |
|----------------|--------------|-------------------|-----------------|--|--|--------------|---------------------------|
| 1 FW | 03/17 (76) | 19:15 | 19:15 | 2.44 | 0.03 | SPE | 30 (ons) |
| 2 AW | 05/29 (149) | 12:22 | 18:12 | 1.55 | 1.8 | IP shock | 27 (haz) |
| 3 FW | 05/31 (151) | 03:18 | 08:58 | 1.1–13.2 | 0.8 | SPE | 7 (ons) |
| 4 AW | 10/26 (299) | 17:54 | 18:31 | 3.1–15.9 | 12. | SPE | 18 (haz) |
| 5 AW | 10/28 (301) | 12:27 | 12:27 | 1.5 | 90 | SPE (bg) | 7 (haz) |
| 6 FW | 10/31 (304) | 06:26 | 13:06 | 1.0–5.9 | (2) | Decline | - |
| 7 AW | 11/02 (306) | 17:26 | 19:19 | 1.0–37.1 | 30 | SPE | 74 (haz) |
| 8 (FW/AW) | 11/04 (308) | 08:32 | (309) 03:05 | 1.0–15.9 | (3),8 | Decline, SPE | - |
| 9 FW | 11/21 (325) | 23:58 | (326) 06:00 | 1.2–6.6 | 0.4 | IP shock | - |

^aGiven are 30–50 MeV protons in (cm² s sr MeV)⁻¹; convert to >30 MeV pfu (hpfu) by applying a factor of 20.

time interval can potentially solve the discrepancy problem for flux decrease periods.

5.3. Evaluation: False and Missed Warnings

[104] In order to issue a warning, the following are required: (1) The actual proton intensity should be below hazard level (here defined as 20 pfu). In order to reduce false warnings from statistical scatter, an average of the previous 2-hour period is required to be under the hazard value. (2) The predicted flux has to exceed hazard level by 50% (value used here: 30 pfu). (3) The predicted value at the time of the warning is required to be the maximum predicted value over the last 2 hours. The blue diamonds represent all the radiation warnings that meet these criteria. Statistically, over the 11 months there have been nine series of SEP hazard warnings issued. Table 3 contains a list of all these 2003 warnings, stating the following:

[105] 1. “Warning Series” is the number of the event in temporal order, including assessment of whether advance warning (AW) of false warning (FW).

[106] 2. “Date in 2003” is the start day of the interval a warning or warning series has been issued.

[107] 3. “Warning Start, UT” is the start of the time interval a warning or warning series has been issued.

[108] 4. “Warning End UT” is the end of the time interval a warning or warning series has been issued.

[109] 5. “Predicted Flux Range” is the predicted flux range in (cm² s sr MeV)⁻¹.

[110] 6. “Observed Peak Flux” is the measured maximum fluxes of the event in (cm² s sr MeV)⁻¹, where applicable.

[111] 7. “Event Type” is the type of event associated with the warning.

[112] 8. “Advance Warning Time” is the advance warning time in minutes from the onset of the proton event (ons) or from proton intensity reaching the hazard level (haz).

[113] For all four SPEs with fluxes exceeding 20 pfu warnings have been issued, all of which happening in the framework of the Halloween storms. Three of the four events, on DOY 299, 301, and 306, clearly have identifiable advance warnings of 18, 7, and 74 min, respectively, before onset of the 50 MeV protons. The fourth event, occurring

on DOY 308, has warnings issued near the onset, but is embedded in a false warning series.

[114] The type of false warning responsible for this is related to the decline of the intensity just below the hazard level of a previous event in close proximity to the onset. Two of these false warning series have been issued (DOY 304 and 308). The forecasting algorithm does not exclude this type of false warning due to the more rapid decline of the measured intensity as compared to the predicted intensity, fulfilling all requirements for a warning. Thus a more sophisticated exclusion scheme has to be developed. From Figure 9 (middle) it is clear that a real warning has indeed been issued before onset of the event on DOY 308.

[115] Note that, remarkably, COSTEP encountered level orange and possible instrument pileup effects at the extreme flux levels throughout the Halloween storms. Despite this fact, the forecasting algorithm is operational, and the predicted fluxes correspond well with the observed ones.

[116] Besides the warning series attributed to intensity declines at the tail end of intense SPEs, only one SPE that is considerably weaker than 20 pfu (3%, or 0.6 pfu) has an advance warning (30 min before onset) associated with it (DOY 76). Another SPE barely misses the hazard level (80%) and has an advance warning (7 min before onset) issued with it.

[117] The remainder of “false” warnings correspond to the encounter with interplanetary shocks that generate significant quantities of low-energy (<30 MeV) energetic storm particles locally. In fact, the event on DOY 149 exceeds the hazard level. In this case, the algorithm even provides an advance warning (27 min before hazard level). These warnings have been anticipated to be rather nowcasts than forecasts, as IP shock particles usually do not show signs of velocity dispersion. This issue might have to be readdressed, owing the positive result. It is likely that relativistic electrons have been quasi-trapped in the upstream foreshock region of the IP shock. Unfortunately, the statistical certainty for this type of warning is too insignificant for making generalizations at this point. A second, below hazard level IP shock event, on DOY 326, has also a warning issued with it.

[118] The bottom plot illustrates the strength of this technique by showing one example of the actual warning time as the delay between proton flux forecast and observed. In this particular event, the warning time is on the order of 20 min, with the forecasting intensity closely resembling the upcoming observations.

6. Discussion and Possible Applications

[119] Several aspects of this study have led to the conclusion that short-term forecasting of solar energetic ions with relativistic electrons is practicable: (1) This study has shown that the onset of <50 MeV protons is always delayed over the onset of relativistic electrons at 1 AU. The average delay time is on the order of 1 hour (63 min). The initial forecasting technique presented, aimed specifically at demonstrating a low miss and false warning rate, provides already on average more than 30 min of advance warning. (2) Moreover, it has been found that the increases in electron and proton intensities are correlated. (3) It has been shown with the superposed epoch technique that on average the maximum intensities of electrons order when events are sorted with the maximum observed proton intensity. (4) An average proton event profile has been shown in which the proton intensities of up to 66 hours into the event are still ordered by event peak flux. (5) A forecasting technique that is based on electron onset data has been successfully applied for forecasting all major SEP events in 2003. The forecasting attempted has been applied for 1-hour advance predictions with relativistic electron data.

[120] Longer-term forecasting, to the extent of the duration of SEP events (up to 3 days), has been considered. The superposed epoch technique shows average profiles for events that are ordered in intensity for the full duration of the event. A more comprehensive treatment for forecasting the SEP time profile would also take into account the solar longitude of the event's activity, which has not been done here because of the lack of event statistics. It should then be possible to successfully apply long-term forecasting with electron onset observations in the same way as we have shown the 1-hour forecasting. A matrix for this, similar to the one shown in Figure 8, should take into account solar cycle effects on the propagation conditions, such as reservoir building in the inner heliosphere [Dalla *et al.*, 2002], which has considerable influence on the particle fluences at 1 AU.

6.1. Onsets of "Gradual" and "Impulsive" Events

[121] The physical basis for the forecasting technique are newly introduced electron and proton rise parameters $\Phi_e = d(\log_{10}(I_e(t = t_1)/I_e(t = t_0)))/dt$ and $\Phi_p = d(\log_{10}(I_p(t = t_1)/I_p(t = t_0)))/dt$ (see Figure 2). It has been shown that the onset intensity-time profile of electrons and protons can be characterized by exponential functions that correspond to these parameters. Physically, the magnitudes of these parameters for any given event are highly correlated and

largely determined by the magnetic connection distance of the flare location from the foot point of the observer.

[122] A distinction between "gradual" and "impulsive" solar energetic particle events is based on criteria such as the elemental composition and ionic charge state [Reames, 2000, 2001; Cane *et al.*, 2003]. Also, there are apparent distinctions in durations of flares associated with these events [Cane and Reames, 1990]. Nonetheless, the paradigm that particle events from the Sun could be clearly classified as small, "impulsive," flare-accelerated or "gradual," large, and CME-shock accelerated [Reames, 1999] has recently been challenged by new observations. For example, increasing ionic charge state of heavy ions with increasing energies up to and beyond 10 MeV/n observed in "gradual" events [Oetliker *et al.*, 1997; Möbius *et al.*, 1999; Labrador *et al.*, 2003] are reminiscent of the abundance enhancements and ionic charge states in "impulsive" events.

[123] Also recently, Reames and Ng [2004] have shown systematic enhancements of heavy ion abundances in "impulsive" events, with smaller flares showing higher such abundances. Although they mention a bimodal distribution between "impulsive" and "gradual" events in support of the paradigm, it is not out of the question that flares are responsible for high-energy particles in "gradual" events, with decreasing abundances of heavy ions with flare size similar to what has been shown within the distribution of impulsive events. As long as the question of a systematic distinction between SEPs is debated, the terms "gradual" and "impulsive," as they are defined by other authors, will be used here as descriptive without implying any physical distinction.

[124] Although the GOES >10 pfu list is characterized as mainly containing "gradual" events, up to three "impulsive" events identified in Table 1a (events 5, 49, and 61) have contributed [see, e.g., Mason *et al.*, 2004; Kahler, 2005]. In addition, the "impulsive" event list of Reames and Ng [2004] has been analyzed in the search for possible correlations between electron and proton rise parameters and connection distance to the flare for this type of event. The aim has been to search the onset characteristics for any bimodal distributions, or lack thereof. Of 39 "impulsive" events from the Reames and Ng list, up to sixteen have been found to provide sufficient data to be added to the statistical survey. Note that the statistical sample of "impulsive" proton events (5) is severely limited. The main reason for exclusions from analysis has been insufficient maximum energy in protons. 17 of 39 events did not show conspicuous enhancements beyond the threshold of 30 MeV. Other causes include proton background from other events, data gaps (in particular all of September 1998), interference with IP shocks and insufficient accuracy in the onset time. On the other hand, most "impulsive" electron enhancements were sufficiently intense beyond 0.3 MeV to be analyzed. However, identification of flare location, in soft X ray, H alpha or EUV, has been lacking in many of these cases.

[125] Note that the above observation, absence of >30 MeV ions but presence of >0.3 MeV electrons, does not provide a physical distinction of “impulsive” from “gradual” events. The electron-to-proton ratio, as often cited in the literature, should be determined at identical speeds or rigidities, and not, as has been done here, compared at arbitrary energies driven by convenience of data availability or, as here, by the need for relativistic speed (electrons) or harm for exploration (protons).

6.2. Heliospheric Transport

[126] The distribution of the “impulsive” events overlaps with the statistical sample of GOES >10 pfu events (most of them interpreted as “gradual,” although *Mason et al.* [2004] classified three and *Kahler* [2005] one of these as “impulsive”), meaning that rise parameters of electrons and protons are correlated and that steeper rises of electrons and protons are found in better connected events. This suggests that the particle transport in the heliosphere is a dominant factor in the appearance of the onsets of all SEP events measured at 1 AU.

[127] Recently, a comparison of Fe/O ratios at various matching rigidities [*Mason et al.*, 2006] has shown that normalized differential fluxes in SEP events track each other. Previously it was thought that over the course of the event the Fe/O ratio changes. This notion was based on the changing ratio at identical particle speeds. The new finding leads to considering that, after a given Fe/O ratio has been established early in the event, transport, not injection profile, is the dominant mechanism for the Fe/O ratio at 1 AU. Observations of STEREO from distinct longitudes at 1 AU will soon shed light on this issue. The implication for forecasting large solar proton events is that small (“impulsive”) events do not contribute excessively to false warnings as their onset characteristics match the overall distribution of SPEs.

[128] Besides a connection-distance effect, there appear to be two major transport-related influences on the appearance of SEP onsets. One originates from the magnetic sector structure, which has been suggested by *Kallenrode* [1993]. Example 2 in Figure 2 shows that a sector boundary encountered during onset likely has adversely affected the correlation between electron and proton rise parameters.

[129] Second, *Dröge* [2000] has derived the mean free paths (MFP) across rigidities for several events. He has done so by numerically simulating this transport parameter from comparison of observed intensity-time profiles and anisotropies with an injection function. He has found that the average MFP changes from event to event on the order of a factor of 20–50, but maintains a characteristic rigidity-dependent (0.3–300 MV) profile. The order of magnitude (factor >20) of this MFP variability is comparable to the scatter in the rise parameters of ~ 1 MV electrons and ~ 100 MV protons about the regression curve with connection distance. The cause for this event-to-event variation is unknown so far. Note, however, that a subset of four nearly identically connected impulsive events in August 2002

(events 12–15, each about 12 hours apart) shows more limited scattering than the overall distribution. This indicates that the propagation conditions either change on longer terms than 2 days or that they depend predominantly on magnetic field line longitude separations that exceed 30° . In this framework it appears important to note that dropouts in the time-intensity profile of several small “impulsive” events have been reported [*Mazur et al.*, 2000] and explained with intermittent connections to small flaring regions with random walk field lines [*Giacalone et al.*, 2000]. A statistical study of these events, which indicate large MFPs, is lacking so far, but it could shed light on the event-to-event variability in MFPs reported by *Dröge* [2000] that is also suspected to be present in this study.

[130] Specific causes, such as transient structures in the solar wind, would influence temporally and spatially the propagation conditions between the Sun and 1 AU. Even the CME that is associated with the flare itself can change propagation conditions close to the Sun. LASCO sequences have shown CMEs to deflect streamers in their vicinity. Similarly, observations of comet tails with the Solar Mass Ejection Imager (SMEI) [*Keil et al.*, 1996] have shown deflections of the same order of magnitude [*Kuchar et al.*, 2006]. Note also that the 1 May 2000 SEP event (event 6 in Table 1b) appears to have radio burst signatures originating behind the (fast) CME [*Klein and Posner*, 2005]. All of these effects stress the importance of the heliospheric propagation conditions on the character of the particle event at and beyond 1 AU.

6.3. Forecasting Applications and Their Relevance

[131] The estimates for arrival delays of 50 MeV protons are on average 63 min over the first arriving relativistic electrons. An estimate that is based on the assumption that the particles have free access along the interplanetary field line to the observer gives 22 min as the theoretical minimum delay. A statistical analysis of the observed delays is in agreement with this value.

[132] The current strategy tends toward solar maximum periods as the ideal time for space exploration activities, as the highly energetic and nearly impossible to shield against galactic cosmic rays are at a minimum flux level. Instead, at this time higher frequencies and intensities of solar energetic particle events have to be taken into account.

[133] Solar particle events that generate large fluxes of protons and heavy ions below ~ 100 MeV/n are much simpler to shield against, with a manageable mass penalty for exploration vehicles. So far, only a likelihood of a particle event occurrence can be provided of upcoming high intensities of solar energetic ions. The forecasting technique introduced here provides actual measurements of the first signs of the particle events at times when the electromagnetic signatures from the Sun have just arrived. Any such technique provides a critical link between probabilistic and real-time forecasting, and it provides the

early certainty that SEPs have reached open field lines. An average value of up to 63 min alert time before 50 MeV/n ions arrive (minus time necessary for sufficient detection and analysis of arriving relativistic electrons) leaves ample time for humans to hide in shielded or solar event radiation-safe locations or even to abort EVA or lunar surface activities.

[134] This study has analyzed the issue of false and missed warnings from relativistic electron forecasting by employing a simple, automated technique on the observations in 2003. For the entire year of 2003, only (up to) five false warnings have been issued within 11 months. Four out of five particle events that have reached the hazard level in this time frame have been forecast successfully, i.e., with advance warning time.

[135] Only one real false warning that points to a clear problem with this technique has been issued, involving a weak SPE. Three “false” warnings are issued in the framework of radiation hazards, either from an IP shock that this method is not intended for, or from an SPE. Both of which remain just below the hazard level, at 40% and 80%, respectively. For two other warnings, the root causes have been identified which will help in developing strategies for preventing these from reoccurring. Within one of the two latter false warning series, a real hazard warning of the only “missed” hazardous SPE has been embedded. The low false alarm rate and near-zero miss rate demonstrates that the warning technique is feasible.

[136] Several recent studies have shown that the unshielded blood-forming organ dose rate from SPEs increases promptly to values beyond 1 cGy-Eq/hr [e.g., Kim *et al.*, 2005], including one of the forecast Halloween events. In order to mitigate risk without adding significant extra cost in mass and power, presumably a radiation-protective shelter for solar particle event activity will be required for all non-LEO missions. As acute radiation effects set in for any extended exposure to 1 cGy-Eq/hr, a fast warning system is also imperative. Note that even though the total warning time is limited to 1 hour, the total dose saved in an extreme event can well exceed 1cGy-Eq. Any operation outside the pressurized vehicle or station requires time before astronauts can be relocated into a radiation shelter. During this time, typically the intensity of a large SPE continues to rise exponentially. Therefore the total dose saved is proportional to the dose rate at the end of the safety operation, hours after a warning will have been issued.

[137] In order to implement the technique, adequate equipment in form of a relativistic electron detector has to be present. Pending better techniques to come, an in situ warning system for the Earth-Moon system that measures relativistic electrons should be required for all non-LEO human missions [e.g., Cohen *et al.*, 2001; Miroshnichenko 2005]. This is in accordance with the as low as reasonably achievable (ALARA) principle that NASA and other international space agencies adhere to. Radiation risk can be significantly mitigated by applying automated

warnings or alert systems for at least travel to the Moon with a stationary system located at L1 (outside the Earth’s magnetosphere). For manned Mars missions, an in situ detector capable of high-cadence relativistic electron detection needs to be present, as the Earth-related warnings do not provide protection for regions of the heliosphere that drastically differ in magnetic connections to solar activity regions and distinctly vary in transport conditions on the path from the Sun. If the inclusion of in situ warning systems at the manned spacecraft is not economic, an array of detectors on (research or operational) spacecraft at various solar longitudes (e.g., Inner Heliospheric Sentinels and Solar Orbiter, or the concept of Solar Weather Buoys, all of which are embedded in the science plans for the U.S. and European space agencies) can be implemented as a sufficient warning system. This, however, would most likely require a direct relay of a warning signal (at an emergency frequency) from the fleet of spacecraft to be properly protected.

[138] For robotic missions in space, the warning time provided by in situ solar electron monitoring offers a chance for preserving valuable instrumentation and data. Automatic switch off of radiation-sensitive devices can help exceeding their life times for relevant scientific observations. Also, in particular for missions such as Laser Interferometer Space Antenna (LISA) with the need for long-term uninterrupted measurements, measures can be taken to prevent contamination from solar energetic ion events [Sumner *et al.*, 2004; Araújo *et al.*, 2005].

[139] Flux forecasting from other possible techniques, such as solar remote sensing, might have the power for making longer-term forecasts in the future. Currently, however, remote sensing methods have to show whether they can match this method’s accuracy in forecasting SEP onset time and intensity-time profile. This method would be immediately part-time operational if the proper warning software is implemented with the SOHO near-real time data stream. There are caveats concerning the reliability at extreme space weather conditions. SOHO does not constantly provide downlink capabilities which is exacerbated by its current antenna problem. Wind and Polar instrumentation might offer alternatives, although downlink or measurement capability limitations are present here as well. If coordinated between these spacecraft, they could cover a substantial fraction per day with near-real time forecasting. With slight adaptations to lower electron energies it might also be possible to utilize the EPAM instrument on ACE.

[140] As ACE, Wind, Polar and SOHO are ageing spacecraft, there is a need for replacement. The GOES spacecraft are neither in a location nor properly equipped to act as a warning system of the kind described here. The main problem is the need for a devoted and operational SEP warning detector with the attribute to be immune to worst-case scenario particle fluxes.

[141] Scientific assessment of the full extent of energetic particle events based on the findings of this study can be

improved upon with additional data. Further research should be undertaken to analyze the radial dependence of the newly found relationship between the parameters Φ_e , Φ_p , and the connection longitude. With the recent launch of STEREO, but also with the Solar Orbiter, Solar Probe, and Solar Sentinels missions, all potential candidates for future missions into the heliosphere, there might be an opportunity to do so, as this analysis requires the measurement, but also the modeling of the 3-D solar wind and the global heliospheric magnetic field. As a result, the impact of solar energetic particle events on other locations in the heliosphere, such as planets, moons, and asteroids, may be reconstructed.

[142] For historical observations of energetic particles without simultaneous monitoring of solar electromagnetic flare signatures, this study might have some relevance as well. The relationship of connection distance with electron and proton risetime might provide a method to reconstruct the source longitude of solar activity and after-the-fact identification of the associated solar active region.

Appendix A: Analysis of SOHO/COSTEP and GOES 8/SEM SEP Data Problems

[143] This appendix thoroughly discusses measurement problems during the onsets and main phases of SEPs for the two particle detectors SOHO/COSTEP and GOES 8/SEM. Figure 1 shows 12 hours of combined COSTEP and SEM observations around the time of the onset of the major solar energetic particle event on 4 November 2001. This event has been chosen as an example because of its high proton intensity, the highest in terms of maximum flux >10 MeV on the list of events observed in 1996–2002. The top plot shows a 250 keV to 8 MeV electron spectrogram. The spectrogram is color coded according to the intensity scale shown on the right. All electrons measured by COSTEP are at relativistic speeds. A combination of electron energy loss mechanisms in SSDs (bremsstrahlung, straggling) in combination with the 1-min time resolution of COSTEP makes it impossible to observe the small (<3 min) electron velocity dispersion effect of solar event relativistic electrons. These same effects pose even larger challenges and limitations to the onset determination from nonrelativistic electron observations. In solid-state detector telescopes, straggling and energy loss from undetected bremsstrahlung emissions lead to a subset of high-energy electrons to be measured in low-energy channels, mimicking early onsets of low-energy electrons. Lack of and overcorrection of this statistical effect can lead to a false interpretation, but at least to significant uncertainty of electron release time at the Sun. The natural “barrier” of light speed, on the other hand, that relativistic electron observations only provide, makes the method of pinpointing of the electron release time as applied here the most straightforward available.

[144] Energy dispersion of solar energetic protons is readily apparent in the second plot from top, containing the 4–50 MeV proton spectrogram. For statistical reasons,

this spectrogram accumulates data over 2 min for each spectrum. Other studies that use COSTEP observations of solar energetic proton onsets or spectrograms exist. These use velocity dispersion from energetic ion onsets [Posner and Kunow, 2003] and solar radio signatures [Klein and Posner, 2005].

[145] The third, fourth, and fifth plots from the top display intensity-time profiles for protons in three distinct energy ranges. These energy bands are defined by the availability of GOES 8/SEM differential proton channels and bounded by the overlap of energy ranges of GOES 8/SEM with SOHO/COSTEP. The energy bands for SEM (blue) and COSTEP (red) are not identical per se. The technique used here for comparison selects from the PHA-based COSTEP spectrogram data of narrow energy bands (from recorded energy losses) and thus provide a new tool for cross calibration with GOES 8/SEM. Despite the limitations in telemetry it should be regarded as a priority for new energetic particle detectors on space missions that, wherever the need for accurate electron-proton timing or cross calibration with other spacecraft might arise, they provide sufficient quantities of PHA-equivalent data products with their telemetry.

[146] Here, we combined the appropriate energies to approximately emulate SEM proton channels. The exact energy ranges for the time profiles in the third plot are: 4.5–8.9 MeV for COSTEP, 4.2–8.7 MeV for SEM; in the fourth plot: 8.9–15.8 MeV for COSTEP, 8.7–14 MeV for SEM; and in the fifth plot: 15.8–39.8 MeV for COSTEP and 15–40 MeV for SEM. Note that here COSTEP proton data have 2 min and SEM data have 5 min of accumulation time per data point.

[147] In solar energetic particle events, three candidates of ionizing radiation are empirically known to trigger certain internally defined levels, yellow and orange, in COSTEP observations: (1) a high SEP electron intensity, (2) a high SEP (or shock-related, energetic storm particle) proton intensity, and (3) a high single-detector trigger level from solar X rays associated with flares.

[148] Yellow indicates low geometric factor mode, a state that the COSTEP instrument automatically switches into. This mechanism is created in order to cover high-flux periods. The switching off of two ring-shaped front SSD segments, however, opens the anticoincidence shield. Here, low-energy protons can spill over into the COSTEP electron channels. This known contamination is corrected for with pulse height analysis techniques. Furthermore, the intensities are corrected for the changed geometric factor.

[149] COSTEP level orange indicates that the instrument dead time reaches or even exceeds the reliable threshold set by limitations in the electronics. Reaching this threshold does not have any immediate effect on the physical state of operation of the instrument, but is deduced from the measurements after the fact. High frequencies of particle detection can generally lead to inaccuracies in intensity from unaccounted for dead time or electronic

pileup. Most notably, during these times the proton intensities can understate the actual values, and most certainly do as intensities rises far beyond the threshold value. For this reason, we show COSTEP level orange data only for comparison with GOES 8/SEM differential proton channel data in this study. All COSTEP observations during level orange have been exclude from statistical and superposed epoch analyses.

[150] Usually at and after time of flare and electron onset, these states, yellow and orange, can be found. In Figures 1 and 2, the background colors indicate the specific states of the COSTEP sensor. We identified each of these steps with a number identifying the time period. This number is provided in the third plot.

[151] In order to identify X rays in Figure 1, we introduce time profiles of the COSTEP front detector count rate in cts/s alongside the nominal low-energy electron channel in $(\text{cm}^2 \text{ s sr MeV})^{-1}$. The front detector count rate is divided by a factor of 1000 for easier comparison.

[152] We note the following: In periods 1–3, at low proton intensities, the GOES 8/SEM proton data are contaminated with a background from cosmic rays. As an artifact of the applied data correction algorithm, the data continuously show nonzero values (horizontal bounding line in all three GOES channels, but most notably in the 9–15 and 15–40 MeV channels; long-term averages are inaccurate at best) above COSTEP intensities. Under background conditions, COSTEP provides a more accurate representation of the actual quiet time proton intensity.

[153] The first indication of the upcoming particle event on 4 November 2001 is the rising COSTEP front detector count rate in periods 1 and 2, which indicates solar X rays arriving from a flare. (Note that by far not all flares produce energetic particle events.) Clearly, the initial COSTEP level orange at ~ 1620 UT (period 2) is related to this X-ray flare, as the single-detector count rate is a good measure for Compton scattered electrons. The decrease in X-ray intensity in period 3 leads to a recovery into the nominal observing mode for COSTEP. No effect of X rays can be seen here in COSTEP protons or electrons throughout periods 1–3, and GOES 8/SEM protons are not affected either.

[154] The onset of the SEP event is sensed first in relativistic COSTEP electrons (electron spectrogram, top plot, and electron time-intensity profile, bottom plot). Starting in period 3, the background intensity in the COSTEP proton spectrogram seems to disappear. This behavior is an effect of significant numbers of electron detection events that exceed the front detector threshold for uncorrected proton count rates. At large electron-to-proton ratios, the statistics only rarely allows protons of the pre-event background to be pulse height analyzed. However, the average intensities for these periods still accurately reflect the proton background intensity, as the weighting factor to be applied for the statistical sample of

protons PHA words here compensates for the low counting statistics.

[155] Note that all three GOES 8/SEM channels rise early, during period 3, simultaneous with electron onset and the arrival of relativistic protons from this ground level event. Obviously, relativistic particles (GeV protons and MeV electrons) contaminate the MeV GOES proton data at this point. The proton intensity for COSTEP increases quite some time later, in period 4, indicating that the on-the-ground processing of the actively vetoed detector can provide for electrons and GCRs not to contribute to proton count rates.

[156] With the proton onset in period 4, COSTEP enters a second brief interval of level orange, just before switching into low geometry factor mode. The proportionality of front-detector count rate and electron intensity indicates that electrons are primarily responsible for triggering this level. In this period, all three GOES 8/SEM differential flux proton channels falsely show proton intensities above pre-event levels. It is most likely that the two lower-energy proton channels are contaminated by relativistic electrons, whereas the 15–40 MeV proton channel sees with a large geometric factor ions that penetrate its passive shielding (R. Zwickl, personal communication, 2006). The magnitude of uncertainty in SEM data from false early proton onsets is approximately (–)1 hour 30 min for 4–9 MeV, (–)1 hour in 9–15 MeV, and (–)30 min in 15–40 MeV (note that the best accuracy in onset timing from GOES 8/SEM can likely be achieved with the 84–200 MeV proton channel).

[157] COSTEP switching into low geometric factor mode (yellow shading, period 5) suspends the orange level for a brief period. Still during period 5, the second COSTEP proton channel increases, indicating the actual arrival of ~ 15 MeV protons. Note that in period 5 the associated SEM 4–9 and 9–15 MeV proton channels have been corrected with the power law correction algorithm. The result is that no useful proton intensities are generated for some time. This is expressed in these channels suddenly dropping to the background level and not showing any indication of the actual proton onset until ~ 40 min and ~ 30 min late, respectively, where a second false proton onset is manifested. On the other hand, the 15–40 MeV GOES 8/SEM channel shows a continuous increase in “proton” intensities before and through the actual onset (This affects the SEM superposed epoch analysis data shown in Figure 7).

[158] The rise in proton intensities (plus a minor contribution from heavier ions) measured by COSTEP in period 5 lifts the overall count rate beyond the threshold level for orange. At the highest proton energies in this particle event, starting in period 6, the (relatively high) intensities from COSTEP and GOES 8/SEM still show good agreement in all three channels. Although questions remain as of the validity of both data sets at these high intensities, we will use COSTEP onset data throughout this study, since GOES 8/SEM data do not show advanced performance

over COSTEP in any of the used energy channels. This is justified as we focus on onset analysis that dips only marginally into the main phase of solar particle events, where real problems with high count rates, in particular from low-energy energetic storm particles arise.

[159] **Acknowledgments.** SOHO is a mission of international collaboration between NASA and ESA. This study benefited from discussions at the ISSI International Team Meeting “Solar/Heliospheric Sources of Suprathermal/Energetic Particles Through the Solar Cycle” (led by P. Király) in March 2006, at the ACE Science Working Team meeting in April 2006, and at the LWS Strategic Capability Development “Earth-Moon-Mars Radiation Environment Module” (principal investigator N. Schwadron) team meeting in November 2006. I would like to express my sincere gratitude to the referees, but also to J. Burch, M. I. Desai, W. Dröge, B. Heber, and L. Klein for their helpful contributions to this study.

References

- Araújo, H. M., P. Wass, D. Shaul, G. Rochester, and T. J. Sumner (2005), Detailed calculation of test-mass charging in the LISA mission, *Astropart. Phys.*, *22*, 451–469.
- Cane, H. V., and D. V. Reames (1990), The relationship between energetic particles and flare properties for impulsive solar flares, *Astrophys. J. Suppl. Ser.*, *73*, 253–258.
- Cane, H. V., D. V. Reames, and T. T. von Roseninge (1988), The role of interplanetary shocks in the longitude distribution of solar energetic particles, *J. Geophys. Res.*, *93*, 9555–9567.
- Cane, H. V., T. T. von Roseninge, C. M. S. Cohen, and R. A. Mewaldt (2003), Two components in major solar particle events, *Geophys. Res. Lett.*, *30*(12), 8017, doi:10.1029/2002GL016580.
- Cohen, C. M. S., R. A. Mewaldt, A. C. Cummings, R. A. Leske, E. C. Stone, P. L. Slocum, M. E. Wiedenbeck, E. R. Christian, and T. T. von Roseninge (2001), Forecasting the arrival of shock-accelerated solar energetic particles of Earth, *J. Geophys. Res.*, *106*, 20,979–20,984.
- Cucinotta, F. A., J. W. Wilson, and F. F. Badavi (1994), Extension of the BRYNTRN code to monoenergetic light ion beams, *NASA Tech. Pap. TP-3472*.
- Dalla, S., A. Balogh, B. Heber, C. Lopate, and R. B. McKibben (2002), Observation of decay phases of solar energetic particle events at 1 and 5 AU from the Sun, *J. Geophys. Res.*, *107*(A11), 1370, doi:10.1029/2001JA009155.
- Drake, J. F., M. Swisdak, H. Che, and M. A. Shay (2006), Electron acceleration from contracting magnetic islands during reconnection, *Nature*, *443*(7111), 553–556.
- Dröge, W. (2000), The rigidity dependence of solar particle scattering mean free paths, *Astrophys. J.*, *537*, 1073–1079.
- Emslie, A. G., J. A. Miller, and J. C. Brown (2004), An explanation for the different locations of electron and ion acceleration in solar flares, *Astrophys. J.*, *602*, L69–L72.
- Giacalone, J., J. R. Jokipii, and J. E. Mazur (2000), Small-scale gradients and large-scale diffusion of charged particles in the heliospheric magnetic field, *Astrophys. J.*, *532*, L75–L78.
- Haggerty, D. K., E. C. Roelof, and G. M. Simnett (2003), Escaping near-relativistic electron beams from the solar corona, *Adv. Space Res.*, *32*(12), 2673–2678.
- Hoff, J. L., L. W. Townsend, and E. N. Zapp (2004), Interplanetary crew doses and dose equivalents: Variations among different bone marrow and skin sites, *Adv. Space Res.*, *34*(6), 1347–1352, doi:10.1016/j.asr.2003.08.056.
- Kahler, S. W. (2005), Characteristic times of gradual solar energetic particle events and their dependence on associated coronal mass ejection properties, *Astrophys. J.*, *628*, 1014–1022.
- Kallenrode, M. B. (1993), Neutral lines and azimuthal “transport” of solar energetic particles, *J. Geophys. Res.*, *98*, 5573–5591.
- Keil, S. L., R. C. Altrock, S. W. Kahler, B. V. Jackson, A. Buffington, B. L. Hick, G. Simnett, C. Eyles, D. F. Webb, and P. Anderson (1996), The Solar Mass Ejection Imager (SMEI): Development and use in space weather forecasting, in *Solar Drivers of Interplanetary and Terrestrial Disturbances: Proceedings of the 16th International Workshop, National Solar Observatory/Sacramento Peak, Sunspot, New Mexico 88349, USA, 16–20 October 1995, Astron. Soc. Pac. Conf. Ser.*, vol. 95, edited by K. S. Balasubramaniam, S. L. Keil, and R. N. Smartt, pp. 158–166, Astron. Soc. of the Pac., San Francisco, Calif.
- Kim, M.-H. Y., X. Hu, and F. Cucinotta (2005), Effect of shielding materials from SPEs on the lunar and Mars surface, paper presented at 1st Space Exploration Conference: Continuing the Voyage of Discovery, Am. Inst. for Aeron. and Astron., Orlando, Fla.
- Klein, K.-L., and A. Posner (2005), The onset of solar energetic particle events: Prompt release of deka-MeV protons and associated coronal activity, *Astron. Astrophys.*, *438*, 1029–1042, doi:10.1051/0004-6361:20042607.
- Kuchar, T., A. Buffington, T. Howard, C. N. Arge, D. Webb, B. V. Jackson, and P. P. Hick (2006), The evolution of comets in the heliosphere as observed by SMEI, *Eos Trans. AGU*, *87*(52), Fall Meet. Suppl., Abstract SH32-08.
- Kunow, H., G. Wibberenz, G. Green, R. Müller-Mellin, and M.-B. Kallenrode (1991), Energetic particles in the inner solar system, in *Physics of the Inner Heliosphere*, vol. 2, *Particles, Waves, and Turbulence, Phys. Chem. Space*, vol. 21, edited by R. Schwenn and E. Marsch, pp. 243–329, Springer, New York.
- Labrador, A., R. A. Leske, R. A. Mewaldt, E. C. Stone, and T. T. von Roseninge (2003), High energy ionic charge state composition in recent large solar energetic particle events, in *Proceedings of the 28th International Cosmic Ray Conference*, vol. 6, edited by T. Kajita et al., pp. 3269–3272, Universal. Acad., Tokyo.
- Liewer, P., M. Neugebauer, J. G. Luhmann, and T. H. Zurbuchen (2002), Active region and coronal hole sources of solar wind at solar activity maximum, *Eos Trans. AGU*, *83*(47), Fall Meet. Suppl., Abstract SH52A-0459.
- Linker, J. A., Z. Mikić, D. A. Biesecker, R. J. Forsyth, S. E. Gibson, A. J. Lazarus, A. Lecinski, P. Riley, A. Szabo, and B. J. Thompson (1999), Magnetohydrodynamic modeling of the solar corona during Whole Sun Month, *J. Geophys. Res.*, *104*, 9809–9830.
- Marqué, C., A. Posner, and K.-L. Klein (2006), Solar energetic particles and radio-silent fast coronal mass ejections, *Astrophys. J.*, *642*, 1222–1235.
- Mason, G. M., J. E. Mazur, J. R. Dwyer, J. R. Jokipii, R. E. Gold, and S. M. Krimigis (2004), Abundances of heavy and ultraheavy ions in ³He-rich solar flares, *Astrophys. J.*, *606*, 555–564.
- Mason, G. M., M. I. Desai, C. M. S. Cohen, R. A. Mewaldt, E. C. Stone, and J. R. Dwyer (2006), The role of interplanetary scattering in Western Hemisphere large solar energetic particle events, *Astrophys. J.*, *645*, L65–L68.
- Mazur, J. E., G. M. Mason, J. R. Dwyer, J. Giacalone, J. R. Jokipii, and E. C. Stone (2000), Interplanetary magnetic field line mixing deduced from impulsive solar flare particles, *Astrophys. J.*, *532*, L79–L82.
- Mewaldt, R. A., C. M. Cohen, R. A. Leske, A. W. Labrador, G. M. Mason, D. K. Haggerty, M. D. Looper, J. E. Mazur, R. S. Selesnick, and M. I. Desai (2005a), Solar energetic particle composition, energy spectra and timing in the 20 January 2005 particle event, *Eos Trans. AGU*, *86*(52), Fall Meet. Suppl., Abstract SH23A-0320.
- Mewaldt, R. A., C. M. S. Cohen, A. W. Labrador, R. A. Leske, G. M. Mason, M. I. Desai, M. D. Looper, J. E. Mazur, R. S. Selesnick, and D. K. Haggerty (2005b), Proton, helium, and electron spectra during the large solar particle events of October–November 2003, *J. Geophys. Res.*, *110*, A09S18, doi:10.1029/2005JA011038.
- Miroshnichenko, L. I. (2005), Radiation field formation and monitoring beyond LEO, *Adv. Space Res.*, *36*(9), 1742–1748, doi:10.1016/j.asr.2005.04.038.
- Möbius, E., et al. (1999), Energy dependence of the ionic charge state distribution during the November 1997 solar energetic particle event, *Geophys. Res. Lett.*, *26*, 145–148.

- Müller-Mellin, R., et al. (1995), COSTEP—Comprehensive suprathermal and energetic particle analyser, *Sol. Phys.*, 162, 483–504.
- Ness, N. F. (1968), Observed properties of the interplanetary plasma, *Annu. Rev. Astron. Astrophys.*, 6, 79–114.
- Oetliker, M., B. Klecker, D. Hovestadt, G. M. Mason, J. E. Mazur, R. A. Leske, R. A. Mewaldt, J. B. Blake, and M. D. Looper (1997), The ionic charge of solar energetic particles with energies of 0.3–70 MeV per nucleon, *Astrophys. J.*, 477, 495–501.
- Ogilvie, K. W., et al. (1995), SWE, a comprehensive plasma instrument for the Wind spacecraft, *Space Sci. Rev.*, 71, 55–77.
- Parker, E. N. (1958), Dynamics of the interplanetary gas and magnetic fields, *Astrophys. J.*, 128, 664–676.
- Posner, A., and H. Kunow (2003), Energy dispersion in solar ion events over 4 orders of magnitude: SOHO/COSTEP and Wind/STICS, in *Proceedings of the 28th International Cosmic Ray Conference*, vol. 6, edited by T. Kajita et al., pp. 3309–3312, Universal Acad., Tokyo.
- Posner, A., T. H. Zurbuchen, N. A. Schwadron, L. A. Fisk, G. Gloeckler, J. A. Linker, Z. Mikić, and P. Riley (2001), Nature of the boundary between open and closed magnetic field line regions at the Sun revealed by composition data and numerical models, *J. Geophys. Res.*, 106, 15,869–15,879.
- Posner, A., N. A. Schwadron, D. J. McComas, E. C. Roelof, and A. B. Galvin (2004), Suprathermal ions ahead of interplanetary shocks: New observations and critical instrumentation required for future space weather monitoring, *Space Weather*, 2, S10004, doi:10.1029/2004SW000079.
- Reames, D. V. (1999), Particle acceleration at the Sun and in the heliosphere, *Space Sci. Rev.*, 90, 413–491.
- Reames, D. V. (2000), Particle acceleration by CME-driven shock waves, in *Proceedings of 26th International Cosmic Ray Conference ICRC XXVI. Salt Lake City, Utah, 17–25 August, 1999*, edited by B. L. Dingus, D. B. Kieda, and M. H. Salamon, *AIP Conf. Proc.*, 516, 289–300.
- Reames, D. V. (2001), Energetic particle composition, in *Proceedings of the 2001 Joint SOHO/ACE Workshop “Solar and Galactic Composition,”* edited by R. F. Wimmer-Schweingruber, *AIP Conf. Proc.*, 598, 153–164.
- Reames, D. V., and C. K. Ng (2004), Heavy-element abundances in solar energetic particle events, *Astrophys. J.*, 610, 510–522.
- Reames, D. V., L. M. Barbier, and C. K. Ng (1996), The spatial distribution of particles accelerated by coronal mass ejection driven shocks, *Astrophys. J.*, 466, 473–486.
- Schatten, K. H., J. M. Wilcox, and N. F. Ness (1969), A model of interplanetary and coronal fields, *Sol. Phys.*, 6, 442–455.
- Schwadron, N. A., et al. (2006), Earth-Moon-Mars Radiation Environment Module (EMMREM), *IEEEAC Pap. 1001*, version 6, *Inst. of Electr. and Electron. Eng.*, New York.
- Shea, M. A., and D. F. Smart (1990), A summary of major solar proton events, *Sol. Phys.*, 127, 297–320.
- Stephens, D. L., Jr., L. W. Townsend, and J. L. Hoff (2005), Interplanetary crew dose estimates for worst case solar particle events based on historical data for the Carrington flare of 1859, *Acta Astronaut.*, 56(9–12), 969–974.
- Sumner, T. J., H. M. Araújo, D. Davidge, A. Howard, C. Lee, G. Rochester, D. Shaul, and P. Wass (2004), Description of charging/discharging processes of the LISA sensor, *Classical Quantum Gravity*, 21, S597–S602.
- Townsend, L. W., and J. S. Neal (2006), A simple method for solar energetic particle event dose forecasting, *Radiat. Meas.*, 41, 1136–1141.
- Tylka, A. J., C. M. S. Cohen, W. F. Dietrich, M. A. Lee, C. G. MacLennan, R. A. Mewaldt, C. K. Ng, and D. V. Reames (2005), Shock geometry, seed populations, and the origin of variable elemental composition at high energies in large gradual solar particle events, *Astrophys. J.*, 625, 474–495.
- van Hollebeke, M. A. I., L. S. Ma Sung, and F. B. McDonald (1975), The variation of solar proton energy spectra and size distribution with heliolongitude, *Sol. Phys.*, 41, 189–223.
- Wang, Y.-M., and N. Sheeley Jr. (1990), Solar wind speed and coronal flux tube expansion, *Astrophys. J.*, 355, 726–732.
- Wilson, J. W., L. W. Townsend, J. E. Nealy, S. Y. Chun, B. S. Hong, W. W. Buck, S. L. Lamkin, B. D. Ganapole, F. Kahn, and F. A. Cucinotta (1989), BRYNTRN: A baryon transport model, *NASA Tech. Pap. TP-2887*.

A. Posner, Southwest Research Institute, 6220 Culebra Rd., San Antonio, TX 78238-5166, USA. (aposner@swri.org)